SUPPLEMENTAL METHODS

Additional simulations comparing the pooled and traditional association methods

We ran additional simulations that model different distributions of read depth across individuals and across the genome. First, we simulated pooled reads by sampling the number of reads from a Poisson distribution with λ = total number of reads (the Poisson distribution assumes that the mean and the variance of the number of reads are equal). For the traditional non-ASM method, we randomly distributed the number of reads that we sampled across individuals as we did in the previous simulations and then sampled allele/methylation status pairs with replacement for each read from the read's individual.

Since sequencing data are known to be over-dispersed, the number of reads is often modeled as being sampled from a negative binomial instead of Poisson distribution (Anders and Huber 2010). We therefore also sampled the number of reads from a negative binomial distribution. We fit negative binomial parameters to the numbers of reads covering CpGs by finding maximum likelihood values. After sampling a number of reads from the negative binomial distribution, we scaled the number of reads to $\frac{(Num.Reads\ at\ Position)*(Num.Reads\ in\ Simulation)}{Mean\ Num.Reads\ Across\ Positions}$ before sampling. For the traditional non-ASM method, we randomly distributed the post-scaling number of reads that we sampled across individuals as we did in the previous simulations and then sampled allele, methylation status pairs with replacement for each read from the read's individual.

In addition to evaluating the power of each method, we also compared its false positive rate to its true positive rate. We simulated false positives by creating a distribution of reads with the same MAF and MMF as our real distribution but 0.0 correlation between allele and methylation status and sampling reads from that distribution. We ran our true positive and false positive simulations at p-value cutoffs 0.5, 0.1, 0.05, 0.01, 0.005, 0.001, 0.0005, 0.0001, 0.00005, and 0.00001. We did this for all of our Fisher's exact test negative binomial simulations with 100 individuals and all combinations of numbers of reads, effect sizes, MAFs, and MMFs. We generated ROC curves to illustrate our results.

Details of data processing

We trimmed reads using Trim Galore! version 0.2.8 (http://www.bioinformatics.babraham.ac.uk/projects/trim_galore/). We used the default parameters with the exception of --stringency 4, --quality 35, and --paired. These parameter adjustments prevented us from removing ends of reads where only a few bases overlap with the adapter, removed read ends that were not especially high-quality, and forced Trim Galore! to account for our reads being paired-end. We chose these parameters after trying multiple parameter settings on a subset of our data because they enabled the most reads to map uniquely to the genome. Next, we converted all HapMap Phase II (Frazer et al. 2007) and 1000 Genomes Phase I Integrated Version 3 (The 1000 Genomes Project Consortium 2010) single nucleotide polymorphisms (SNPs) with MAF > 0.04 in human genome version hg19 (The International Human Genome Sequencing Consortium 2001) into N's in order to eliminate sources of reference bias when mapping (Degner et al. 2009). We mapped reads to the autosomes in hg19 (The International Human Genome Sequencing Consortium 2001) using Bismark version 0.12.3 (Krueger and Andrews 2011) with Bowtie 2 version 2.2.3 (Langmead and Salzberg 2012). Bismark converts all Cs to Ts and all Gs to As before mapping, maps them to both a C-to-T and a G-to-A-converted genome, and then converts the Ts and As back to their original bases (Krueger and Andrews 2011). We used the default parameters with the exception of, for mapping, --bowtie2 and, for extracting methylation, --ignore_r2 7, -p, and --no_overlap so that we could remove incorrect methylation calls at the 5' end of read 2 due to DNA repair (Supplemental Figure 27), account for our reads being paired-end, and not double-count cytosines on both ends of the reads. In addition, when calling methylation statuses, we removed the 11 bases at the 3' end of read one and the 31 bases at the 3' end of read two because we noticed substantial methylation degradation towards the 3' end that seemed independent of read sequence (Supplemental Figure 27). We also used Bismark (Krueger and Andrews 2011) to map reads to the lambda phage genome (Leinonen et al. 2011) and to evaluate the observed methylation; since lambda phage is completely unmethylated, any observed methylation is due to failure in bisulfite treatment or sequencing errors.

We also filtered the reads in multiple ways. Bismark divides all cytosines into four categories: cytosines followed by guanines (CpGs), cytosines followed by non-guanines followed by guanines (CHGs), cytosines followed by at least two non-guanines (CHHs), and cytosines followed by Ns (CNs). For our analysis, we focused on CpGs. The CpGs with called methylation statuses should not contain most SNPs because we masked SNPs with Ns, so such CpGs would have become CNs. After running Bismark, we removed duplicates from the mapped reads using rmdup from Samtools version 0.1.19 (Li et al. 2009). We also removed reads that overlapped with regions in the ENCODE black list (The ENCODE Project Consortium 2012). Thus, we were left with reliable mapped reads and methylation calls.

After removing duplicates, we determined the allele of each SNP, insertion, and deletion from 1000 Genomes AFR in each read (The 1000 Genomes Project Consortium, 2010). We used only the 1000 Genomes AFR variants because calling variants from pooled data is a challenging problem (Nielsen et al. 2011; Li 2014), and this panel should contain most of the variants in these individuals (The 1000 Genomes Project Consortium, 2010); however, when genomic variant positions are not available, they can also be inferred from the reads using established methods like GATK (McKenna et al. 2010) or Bis-SNP (Liu et al. 2012). When identifying alleles from reads, we did not include any cytosine/thymine (C/T) SNPs or adenine/guanine (A/G) SNPs. During the bisulfite treatment, unmethylated cytosines are converted into uracils (that become thymines during PCR) and, as a result, the guanines that complement them become adenines during PCR. Therefore, for C/T SNPs, we cannot distinguish between unmethylated cytosines and thymines from the original reads, and for A/G SNPs on the reverse strand, we cannot distinguish between adenines that complement unmethylated cytosines (that have become thymines) and adenines from the original reads.

Estimating the fraction of each individual in the pool

Although unnecessary for our method, we evaluated how well our pool represented each individual by using our reads to estimate the frequency of each individual in our pool. In order to do this, we first computed the number of reads covering each allele of each SNP from HapMap Phase II (Frazer et al. 2007). We then solved the constrained optimization problem

$$\mathrm{argmin}_f \frac{1}{2}(Xf-y)^2$$

subject to

$$f \geq 0$$

$$\sum_j^{60} f_j \ = 1,$$

where y is the weighted vector of alternate allele frequencies in the pool, f is the vector of individual frequencies in the pool, f_j is the entry in the vector f for individual j, and X is a weighted (number of variants) x (number of individuals) matrix of genotypes (on a 0 to 1 scale, where 0 is homozygous reference allele, 0.5 is heterozygous, and 1 is homozygous alternate allele) of each individual for each SNP. We weighted y and X by multiplying them by the number of reads at the current SNP and then dividing them by the sum of the numbers of reads across all SNPs; this allows SNPs with more reads to contribute more to the optimization. We solved the optimization problem using Matlab's lsqlin (Coleman and Li 1996) with initial individual frequencies of 1/60. We should note that this does require genotype information, which may not always be available for pooled samples, but the results from this are not necessary for our pooling method.

Obtaining data for overlaps between mQTLs, eQTLs, dsQTLs, CTCF-binding-QTLs, and GWAS hits

For eQTLs from Pickrell *et al.*, we downloaded the final_eqtl_list, and final_sqtl_list files from eqtl.uchicago.edu/RNA_Seq_data/results (Pickrell et al. 2010). For eQTLs from the Geuvadis Consortium, a larger, more recent study, we downloaded the YRI89 files from ftp://ftp.ebi.ac.uk/pub/databases/microarray/data/experiment/GEUV/E-GEUV-1/analysis_results; for SNPs that were tested for eQTLs in Geuvadis YRI, we downloaded data from http://ftp.1000genomes.ebi.ac.uk/vol1/ftp/release/20130502 (Lappalainen et al. 2013). For dsQTLs, we downloaded the files from eqtl.uchicago.edu/dsQTL_data/QTLs; for SNPs that were tested for dsQTLs, we downloaded data from http://eqtl.uchicago.edu/dsQTL_data/GENOTYPES (Degner et al. 2012). We then used liftOver (Kent et al. 2002) to convert the SNP coordinates from hg18 to hg19 and finally combined short-range and long-range dsQTLs. For CTCF-binding-QTLs and SNPs that were tested for CTCF-binding-QTLs, we downloaded data from http://www.ebi.ac.uk/birney-srv/CTCF-QTL (Ding et al. 2014). For the GWAS data, we downloaded the GWAS Catalog (Welter et al. 2014) on January 14, 2014. For all QTL and GWAS datasets except for the CTCF-binding-QTLs, we used SNAP Proxy Search (Johnson et al. 2008) with the YRI population panel and the default distance limit to identify 1000 Genomes Pilot 1 YRI SNPs in perfect LD and r^2 ≥ 0.8 LD with the SNPs in the dataset and used liftOver (Kent et al. 2002) to convert SNP coordinates from hg18 to hg19. For the CTCF-binding-QTLs, we used the same procedure for finding SNPs in LD as was used in the other studies except that we used SNAP's CEU population panel (Johnson et al. 2008) because this study was done in individuals with European ancestry; we used this study even though it came from a different population because it is the only existing CTCF-binding-QTL study.

Obtaining mQTLs from the Zhang et al. data

We compared our mQTLs to those in the Zhang *et al.* study because it is one of the two largest CpG microarray studies of Yoruban LCLs (Zhang et al. 2014). We obtained a list of filtered CpGs from the authors, where the filtering included all of the metrics described in their paper. We downloaded their Supplemental Table 2, which has their YRI mQTLs. We computed the p-value for the overlap between CpGs with mQTLs in both studies using a hypergeometric test, where the background was all CpGs tested in both studies.

Obtaining mQTLs from the Banovich et al. data

We also compared our mQTLs to those in the Banovich *et al.* study because it is the other of the two largest CpG microarray studies of Yoruban LCLs (Banovich et al. 2014). We obtained a list of filtered CpGs from the authors, where the filtering included all of the metrics described in their paper. We downloaded their mQTLs from http://giladlab.uchicago.edu/data/meQTL_summary_table.txt (Banovich et al. 2014). We computed the p-value for the overlap between CpGs with mQTLs in both studies using a hypergeometric test, where the background was all CpGs tested in both studies. We also intersected their CpGs with mQTLs with those found by Zhang et al. (Zhang et al. 2014) to compare the results of these two earlier studies.

Overlapping CpGs in our study with CpG islands and surrounding regions

We determined the fraction of CpGs with mQTLs in our data-set that are also in CpG islands or shores. We did this by downloading CpG islands from http://rafalab.jhsph.edu/CGI/model-based-cpg-islands-hg19.txt (Irizarry et al. 2009; Wu et al. 2010). Because CpG shores are generally defined as the 2 kb surrounding CpG islands in each direction (Price et al. 2013), we extended each CpG island by 2 kb in each direction using BEDTools slopBed version 2.16.1 (Quinlan and Hall 2010). We then identified the number of CpGs with mQTLs that are in both the CpG islands and the extended CpG islands.

SUPPLEMENTARY REFERENCES

Anders S, Huber W. 2010. Differential expression analysis for sequence count data. *Genome Biol* **11**: R106.

Coleman TF, Li Y. 1996. A Reflective Newton Method for Minimizing a Quadratic Function Subject to Bounds on Some of the Variables. *SIAM J Optim* **6**: 1040–1058.

Degner JF, Marioni JC, Pai AA, Pickrell JK, Nkadori E, Gilad Y, Pritchard JK. 2009. Effect of read-mapping biases on detecting allele-specific expression from RNA-sequencing data. *Bioinformatics* **25**: 3207–3212.

Degner JF, Pai AA, Pique-Regi R, Veyrieras J-B, Gaffney DJ, Pickrell JK, De Leon S, Michelini K, Lewellen N, Crawford GE, et al. 2012. DNase I sensitivity QTLs are a major determinant of human expression variation. *Nature* **482**: 390–394.

Ding Z, Ni Y, Timmer SW, Lee B-K, Battenhouse A, Louzada S, Yang F, Dunham I, Crawford GE, Lieb JD, et al. 2014. Quantitative Genetics of CTCF Binding Reveal Local Sequence Effects and Different Modes of X-Chromosome Association. *PLoS Genet* **10**: e1004798.

Frazer KA, Ballinger DG, Cox DR, Hinds DA, Stuve LL, Gibbs RA, Belmont JW, Boudreau A, Hardenbol P, Leal SM, et al. 2007. A second generation human haplotype map of over 3.1 million SNPs. *Nature* **449**: 851–861.

Johnson AD, Handsaker RE, Pulit SL, Nizzari MM, O'Donnell CJ, de Bakker PIW. 2008. SNAP: a web-based tool for identification and annotation of proxy SNPs using HapMap. *Bioinformatics* **24**: 2938–2939.

Kent WJ, Sugnet CW, Furey TS, Roskin KM, Pringle TH, Zahler AM, Haussler D. 2002. The Human Genome Browser at UCSC. *Genome Res* **12**: 996–1006.

Krueger F, Andrews SR. 2011. Bismark: a flexible aligner and methylation caller for Bisulfite-Seq applications. *Bioinformatics* **27**: 1571–1572.

Langmead B, Salzberg SL. 2012. Fast gapped-read alignment with Bowtie 2. *Nat Methods* **9**: 357–359.

Lappalainen T, Sammeth M, Friedländer MR, 't Hoen P a C, Monlong J, Rivas MA, Gonzàlez-Porta M, Kurbatova N, Griebel T, Ferreira PG, et al. 2013. Transcriptome and genome sequencing uncovers functional variation in humans. *Nature* **501**: 506–511.

Leinonen R, Akhtar R, Birney E, Bower L, Cerdeno-Tárraga A, Cheng Y, Cleland I, Faruque N, Goodgame N, Gibson R, et al. 2011. The European Nucleotide Archive. *Nucleic Acids Res* **39**: D28–D31.

Li H. 2014. Toward better understanding of artifacts in variant calling from high-coverage samples. *Bioinformatics* **30**: 2843-2851.

Li H, Handsaker B, Wysoker A, Fennell T, Ruan J, Homer N, Marth G, Abecasis G, Durbin R. 2009. The Sequence Alignment/Map format and SAMtools. *Bioinformatics* **25**: 2078–2079.

Liu Y, Siegmund KD, Laird PW, Berman BP. 2012. Bis-SNP: Combined DNA methylation and SNP calling for Bisulfite-seq data. *Genome Biol* **13**: R61.

Nielsen R, Paul JS, Albrechtsen A, Song YS. 2011. Genotype and SNP calling from next-generation sequencing data. *Nat Rev Genet* **12**: 443–451.

Pickrell JK, Marioni JC, Pai AA, Degner JF, Engelhardt BE, Nkadori E, Veyrieras J-B, Stephens M, Gilad Y, Pritchard JK. 2010. Understanding mechanisms underlying human gene expression variation with RNA sequencing. *Nature* **464**: 768–772.

The 1000 Genomes Project Consortium. 2010. A map of human genome variation from population-scale sequencing. Nature **467**: 1061-1073.

The ENCODE Project Consortium. 2012. An integrated encyclopedia of DNA elements in the human genome. *Nature* **489**: 57–74.

The International Human Genome Sequencing Consortium. 2001. Initial sequencing and analysis of the human genome. *Nature* **409**: 860–921.

Welter D, MacArthur J, Morales J, Burdett T, Hall P, Junkins H, Klemm A, Flicek P, Manolio T, Hindorff L, et al. 2014. The NHGRI GWAS Catalog, a curated resource of SNP-trait associations. *Nucleic Acids Res* **42**: D1001–D1006.

Supplemental Figure 1: Pooled ASM vs. traditional non-ASM method, zero-variance simulations

Plots showing the correlation of the allele and methylation status versus the fraction of simulations that identify the mQTL with p-value < 0.001 for 40, 160, and 640 reads. In the simulations for this figure, the reads are randomly sampled with replacement from the pool/individuals, meaning that, for each read, we select an allele-methylation status combination from the distribution of combinations in our pool/for the individual. There are 100 individuals, and there are 0.1 minor allele and minor methylation status frequencies. The reads from the pool are randomly distributed across the individuals, so that each individual has approximately (but not exactly) the same number of reads.

Supplemental Figure 2: Pooled ASM vs. traditional non-ASM method, Poisson distribution simulations

Plots showing the correlation of the allele and methylation status versus the fraction of simulations that identify the mQTL with p-value < 0.001 for 40, 160, and 640 reads. In the simulations for this figure, reads are sampled from a Poisson distribution, there are 100 individuals, and there are 0.1 minor allele and minor methylation status frequencies.

Supplemental Figure 3: Pooled ASM vs. traditional non-ASM method, F-test p-value simulations

Plots showing the correlation of the allele and methylation status versus the fraction of simulations that identify the mQTL with p-value < 0.001 for 40, 160, and 640 reads. In the simulations for this figure, reads are sampled from a negative binomial distribution, there are 100 individuals, and there are 0.1 minor allele and minor methylation status frequencies. p-values for mQTLs were calculated using the p-value from the F-test for the regression that predicts methylation status as a function of allele/genotype instead of Fisher’s Exact Test.

Supplemental Figure 4: Pooled ASM vs. traditional non-ASM method, correlation p-value simulations

Plots showing the correlation of the allele and methylation status versus the fraction of simulations that identify the mQTL with p-value < 0.001 for 40, 160, and 640 reads. In the simulations for this figure, reads are sampled from a negative binomial distribution, there are 100 individuals, and there are 0.1 minor allele and minor methylation status frequencies. p-values for mQTLs were calculated using the asymptotic p-value from the Pearson correlation instead of Fisher’s Exact Test.

Supplemental Figure 5: Pooled ASM vs. traditional non-ASM method, MAF = 0.3 simulations

Plots showing the correlation of the allele and methylation status versus the fraction of simulations that identify the mQTL with p-value < 0.001 for 40, 160, and 640 reads. In the simulations for this figure, reads are sampled from a negative binomial distribution, there are 100 individuals, and there are 0.3 minor allele and minor methylation status frequencies.

Supplemental Figure 6: Pooled ASM vs. traditional non-ASM method, MAF = 0.5 simulations

Plots showing the correlation of the allele and methylation status versus the fraction of simulations that identify the mQTL with p-value < 0.001 for 40, 160, and 640 reads. In the simulations for this figure, reads are sampled from a negative binomial distribution, there are 100 individuals, and there are 0.5 minor allele and minor methylation status frequencies.

Supplemental Figure 7: Pooled ASM vs. traditional non-ASM method, 25 individuals simulations

Plots showing the correlation of the allele and methylation status versus the fraction of simulations that identify the mQTL with p-value < 0.001 for 40, 160, and 640 reads. In the simulations for this figure, reads are sampled from a negative binomial distribution, there are 25 individuals, and there are 0.1 minor allele and minor methylation status frequencies.

Supplemental Figure 8: Pooled ASM vs. traditional non-ASM method, 400 individuals simulations

Plots showing the correlation of the allele and methylation status versus the fraction of simulations that identify the mQTL with p-value < 0.001 for 40, 160, and 640 reads. In the simulations for this figure, reads are sampled from a negative binomial distribution, there are 400 individuals, and there are 0.1 minor allele and minor methylation status frequencies.

Supplemental Figure 9: ROCs for pooled ASM vs. traditional non-ASM method, MAF = 0.1 simulations

ROC curves comparing the false positive versus true positive rates for simulations for 40, 160, and 640 reads and effect sizes 1.0 and 0.5. In the simulations for this figure, reads are sampled from a negative binomial distribution, there are 100 individuals, and there are 0.1 minor allele and minor methylation status frequencies.

Supplemental Figure 10: ROCs for pooled ASM vs. traditional non-ASM method, F-test simulations

ROC curves comparing the false positive versus true positive rates for simulations for 40, 160, and 640 reads and effect sizes 1.0 and 0.5. In the simulations for this figure, reads are sampled from a negative binomial distribution, there are 100 individuals, and there are 0.1 minor allele and minor methylation status frequencies. p-values for mQTLs were calculated using the p-value from the F-test for the regression that predicts methylation status as a function of allele/genotype instead of Fisher's Exact Test.

Supplemental Figure 11: ROCs for pooled ASM vs. traditional non-ASM method, MAF = 0.3 simulations

ROC curves comparing the false positive versus true positive rates for simulations for 40, 160, and 640 reads and effect sizes 1.0 and 0.5. In the simulations for this figure, reads are sampled from a negative binomial distribution, there are 100 individuals, and there are 0.3 minor allele and minor methylation status frequencies.

Supplemental Figure 12: ROCs for pooled ASM vs. traditional non-ASM method, MAF = 0.5 simulations

ROC curves comparing the false positive versus true positive rates for simulations for 40, 160, and 640 reads and effect sizes 1.0 and 0.5. In the simulations for this figure, reads are sampled from a negative binomial distribution, there are 100 individuals, and there are 0.5 minor allele and minor methylation status frequencies.

Supplemental Figure 13: p-Values from pooled ASM vs. traditional non-ASM method simulations

Histograms of p-values for variant-CpG pairs from 10,000 simulations. These simulations were done for 40 reads, perfect correlation between allele and methylation status, 0.1 minor allele and methylation status frequencies, and 100 individuals. The number of reads in each simulation was sampled from a negative binomial distribution, and p-values were computed using Fisher's Exact Test. **a)** $-\log_{10}$p-values for pooling method. **b)** $-\log_{10}$p-values for traditional method.

Supplemental Figure 14: Estimated fraction of each individual's DNA in the pool

Supplemental Figure 15: Distances between variants and corresponding CpGs for mQTLs

Supplemental Figure 16: Pyrosequencing validation of an mQTL that is in strong LD with a GWAS hit

Shown is an mQTL involving a SNP in 0.80 LD with a SNP previously associated with basal cell carcinoma that was validated in a different set of 30 LCLs. **a)** Pooled bisulfite sequencing for the mQTL showing strong association. **b)** Pyrosequencing validation of the mQTL in 30 additional YRI individuals did not confirm our findings. Light blue points are the methylation percentages from individuals, and crosses are the mean methylation percentages for individuals of each genotype.

Supplemental Figure 17: Pyrosequencing validation of an mQTL that is a dsQTL

Shown is an mQTL involving a SNP previously associated with open chromatin that was validated in a different set of 30 LCLs. **a)** Pooled bisulfite sequencing for the mQTL, showing strong association. **b)** Pyrosequencing validation of the mQTL in 30 additional YRI individuals shows that the mQTL is not limited to the individuals in our study. Light blue points are the methylation percentages from individuals, and crosses are the mean methylation percentages for individuals of each genotype.

Supplemental Figure 18: Pyrosequencing validation of an mQTL that is in strong LD with a GWAS hit

Shown is an mQTL involving a SNP in 0.84 LD with a SNP previously associated with hypertension risk in short sleep duration that was validated in a different set of 30 LCLs. **a)** Pooled bisulfite sequencing for the mQTL, showing strong association. **b)** Pyrosequencing validation of the mQTL in 30 additional YRI individuals shows that the mQTL is not limited to the individuals in our study. Light blue points are the methylation percentages from individuals, and crosses are the mean methylation percentages for individuals of each genotype.

Supplemental Figure 19: Pyrosequencing validation of an mQTL that is in perfect LD with a GWAS hit

Shown is an mQTL involving a SNP in perfect LD with a SNP previously associated with venous thromboembolism that was validated in a different set of 30 LCLs. **a)** Pooled bisulfite sequencing for the mQTL, showing strong association. **b)** Pyrosequencing validation of the mQTL in 30 additional YRI individuals shows that the mQTL is not limited to the individuals in our study. Light blue points are the methylation percentages from individuals, and crosses are the mean methylation percentages for individuals of each genotype.

Supplemental Figure 20: Pyrosequencing validation of an mQTL that is in strong LD with a GWAS hit

Shown is an mQTL involving a SNP in 0.86 LD with a SNP previously associated with prostate cancer that was validated in a different set of 30 LCLs. **a)** Pooled bisulfite sequencing for the mQTL, showing strong association. **b)** Pyrosequencing validation of the mQTL in 30 additional YRI individuals shows that the mQTL is not limited to the individuals in our study. Light blue points are the methylation percentages from individuals, and crosses are the mean methylation percentages for individuals of each genotype.

Supplemental Figure 21: Pyrosequencing validation of an mQTL that is an exon-level eQTL

Shown is an mQTL involving a SNP previously associated with exon-level expression that was validated in a different set of 30 LCLs. **a)** Pooled bisulfite sequencing for the mQTL, showing strong association. **b)** Pyrosequencing validation of the mQTL in 30 additional YRI individuals shows that the mQTL is not limited to the individuals in our study. Light blue points are the methylation percentages from individuals, and crosses are the mean methylation percentages for individuals of each genotype.

Supplemental Figure 22: Numbers of tested CpGs and mQTLs in pooled vs. Zhang *et al*. dataset

a) Illustration of the number of CpGs tested for mQTLs in our pooled dataset and in the Zhang *et al*. array data-set. **b)** Illustration of the number of CpGs with mQTLs in our pooled dataset and in the Zhang *et al*. array data-set.

Supplemental Figure 23: Numbers of tested CpGs and mQTLs in pooled vs. Banovich *et al*. dataset

a) Illustration of the number of CpGs tested for mQTLs in our pooled dataset and in the Banovich *et al*. array data-set. **b)** Illustration of the number of CpGs with mQTLs in our pooled data-set and in the Banovich *et al*. array dataset.

Supplemental Figure 24: Fold-enrichments of CpGs with mQTLs in each chromatin state

Numbers of chromatin states correspond to the numbers listed in Table 1.

Supplemental Figure 25: p-Values for mQTL enrichment in open chromatin from LCLs vs. others

Histograms of $-\log_{10}$p-values for mQTL enrichment in open chromatin regions from different cell types. The histogram for LCLs is in red, and the histogram for all other cell types is in light blue.

Supplemental Figure 26: Fold-enrichments of mQTLs in TF-binding sites

This bar graph contains the 12 TF-binding sites that are enriched for mQTLs in Supplementary Table 1.

Supplemental Figure 27: Methylation bias that depends on position in read

M-bias plots generated by Bismark for one library in one sequencing lane of one flowcell. The dark blue line in the plot is the percentage of CpG methylation. The part of the read underlined by the dark blue line was removed during methylation status calling using Bismark's bismark_methylation_extractor's ignore_r2 option. The parts of the reads underlined by the dark red lines were removed during methylation status calling by in-house scripts. Other libraries and sequencing lanes and flowcells for this library have M-bias plots that look similar to this one.

Supplemental Figure 28: Using LD to combine data from reads with the same CpG

Reads for each variant, CpG pair can be used to generate a contingency table, even though the individual from which each read was generated is not known. Reads from the same CpG that have different variants that are in perfect LD can be combined, and the alleles of the first variant for reads with the second variant can be imputed when making the contingency table.

Supplemental Figure 1

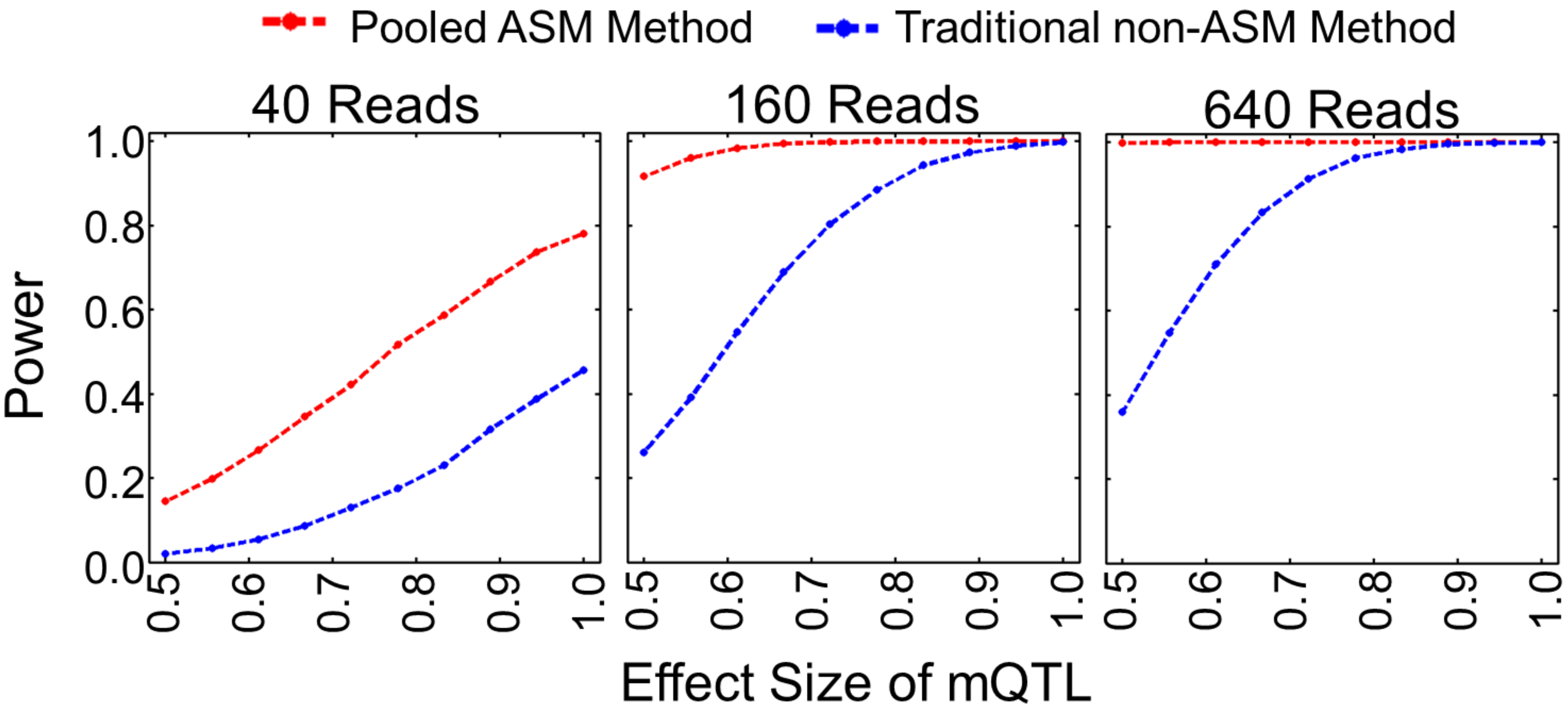

Supplemental Figure 2

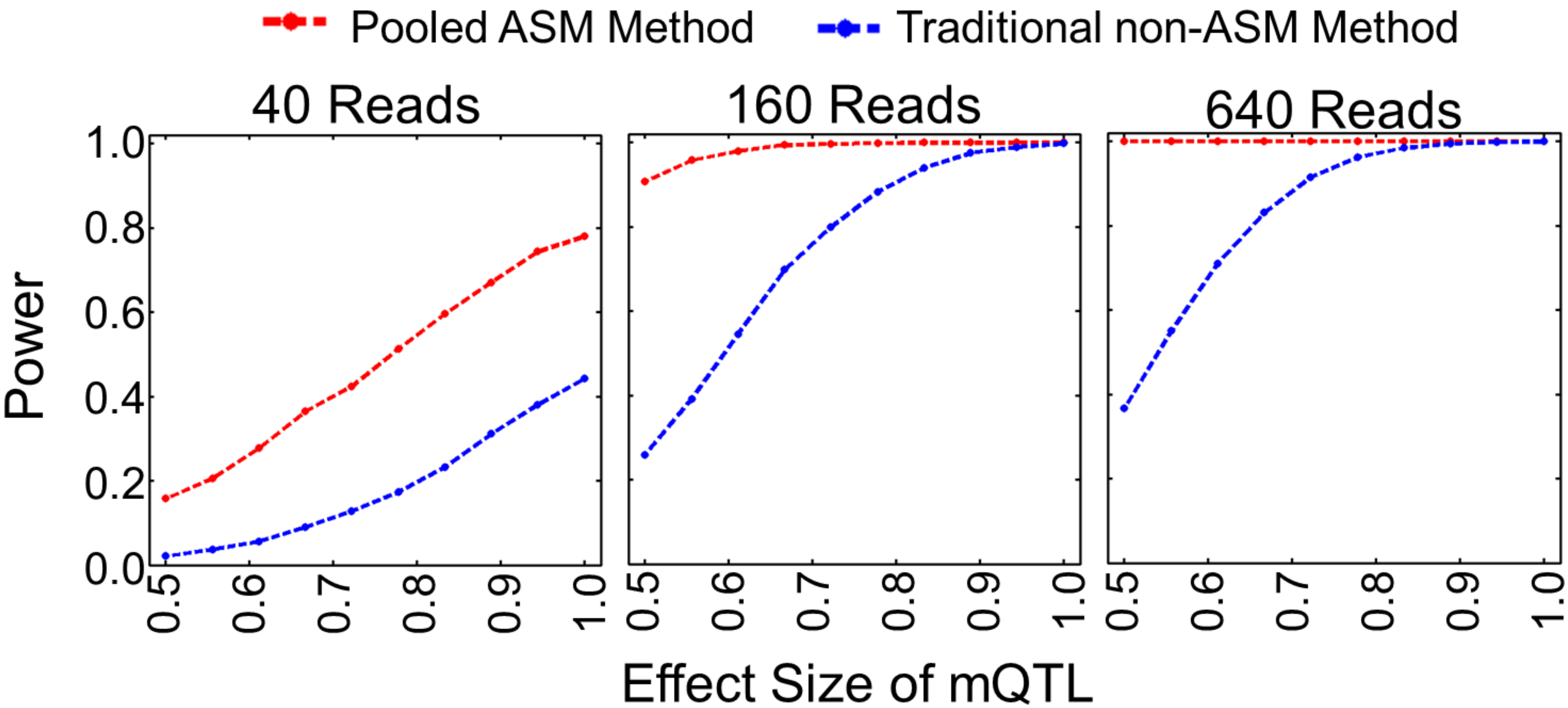

Supplemental Figure 3

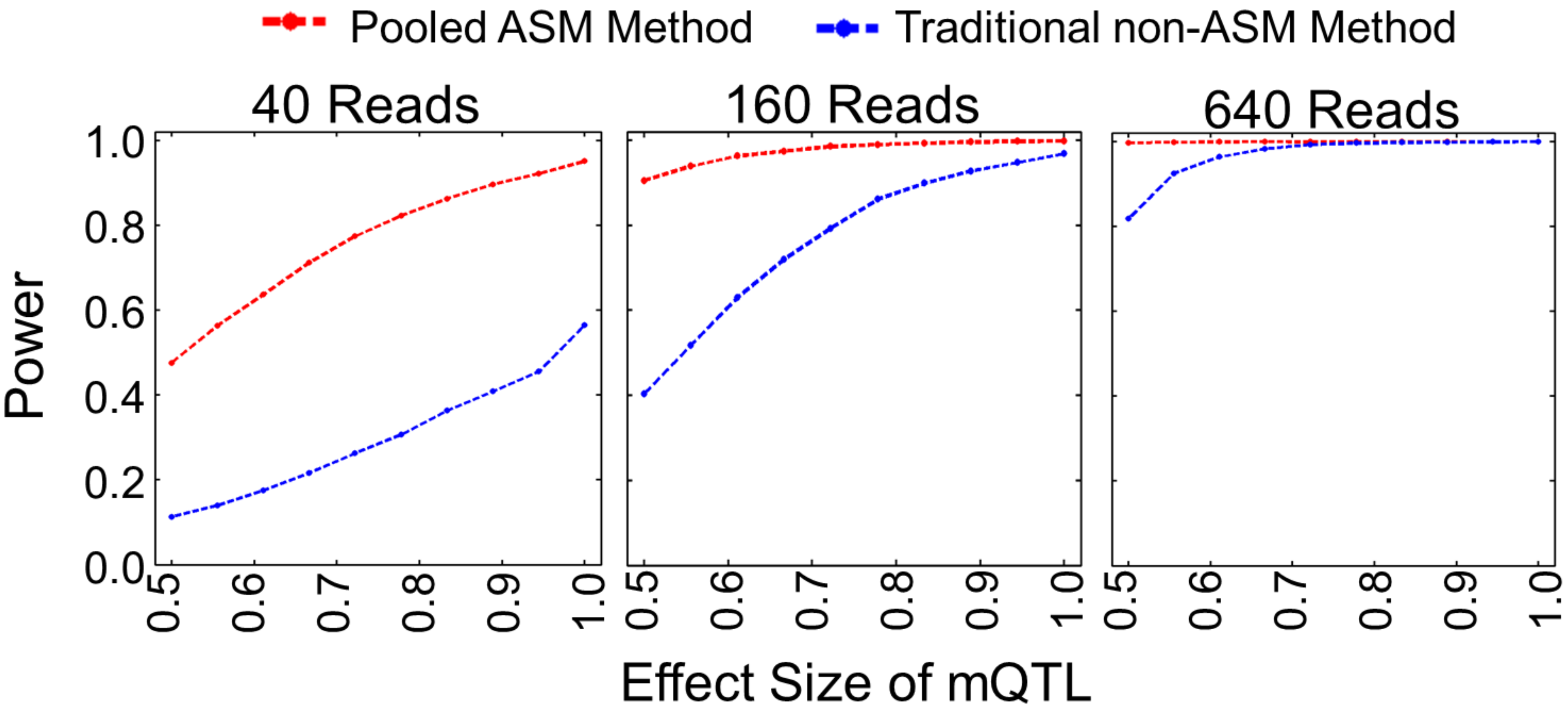

Supplemental Figure 4

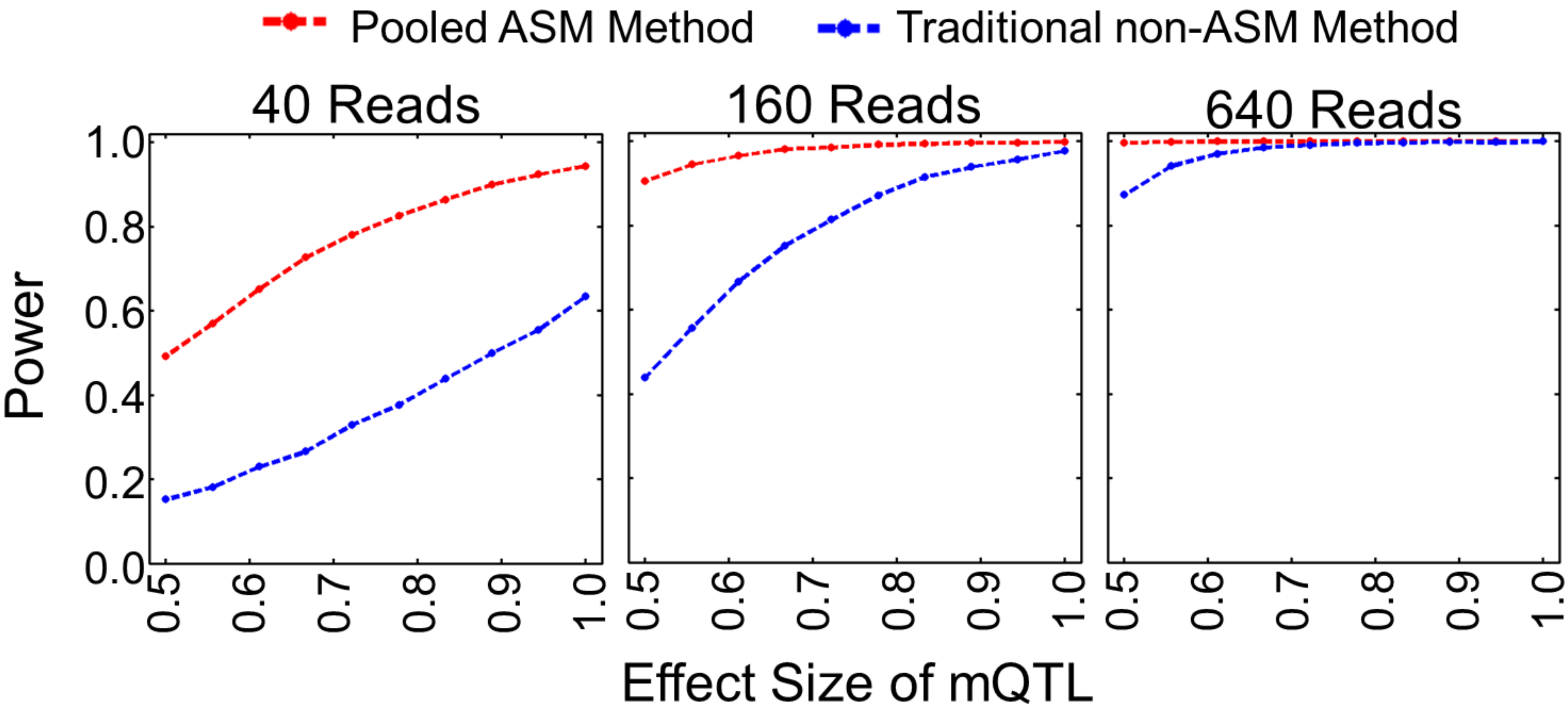

Supplemental Figure 5

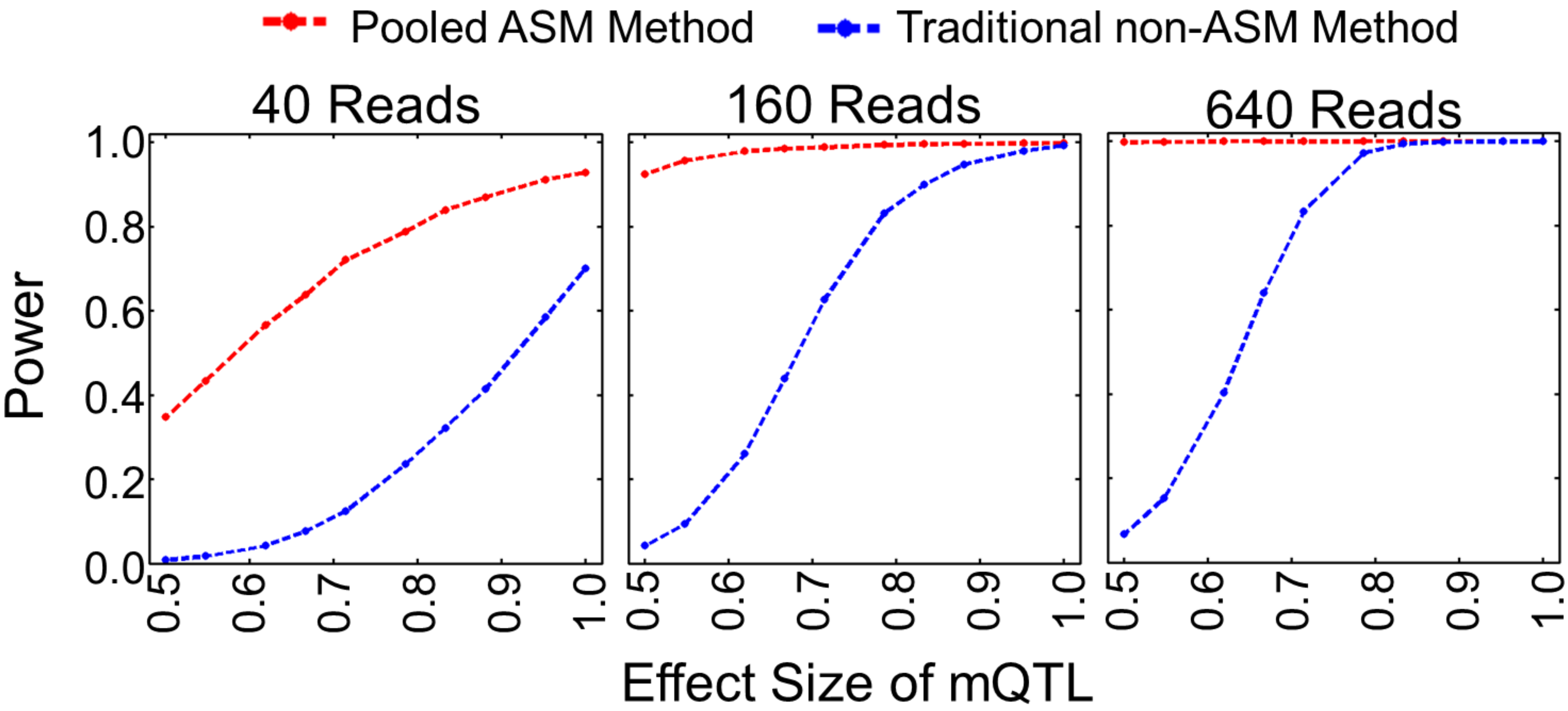

Supplemental Figure 6

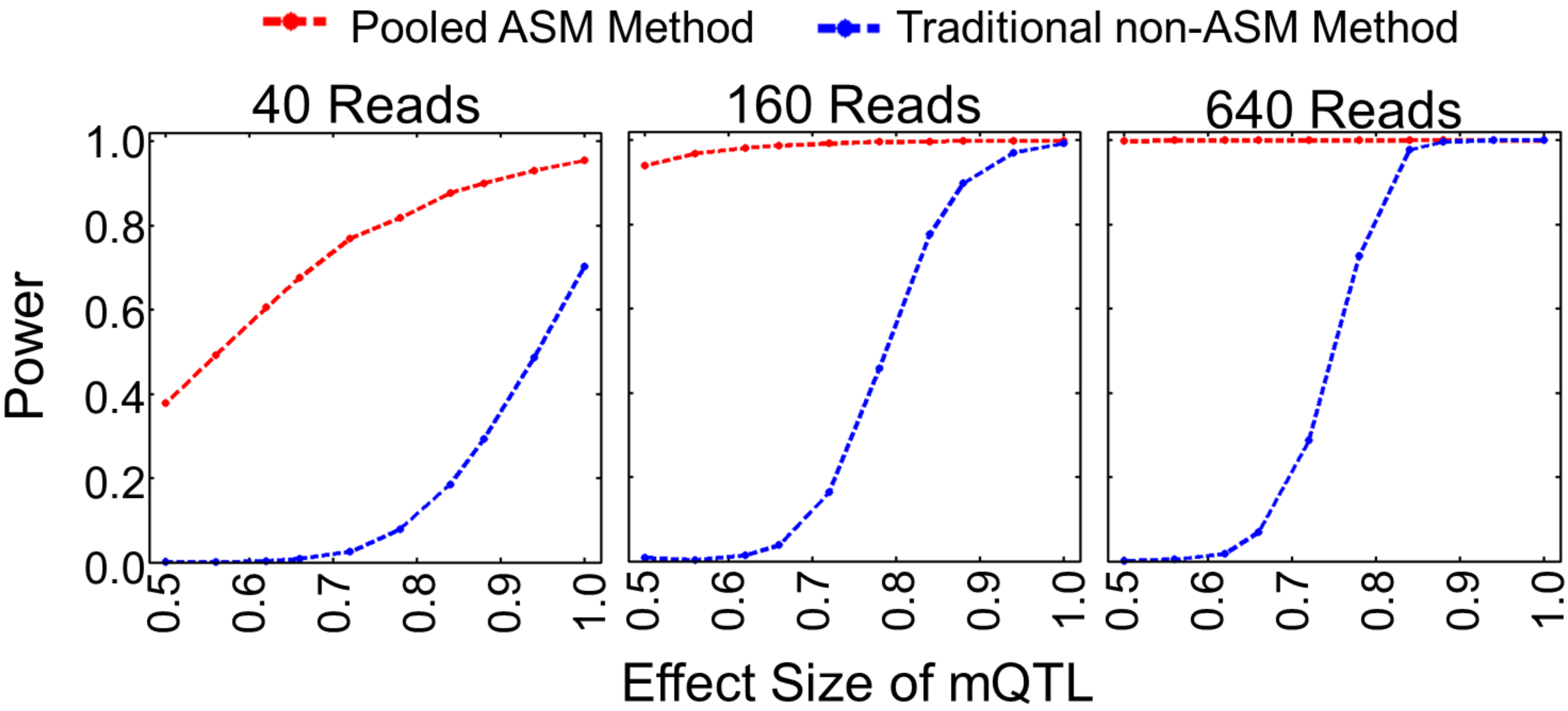

Supplemental Figure 7

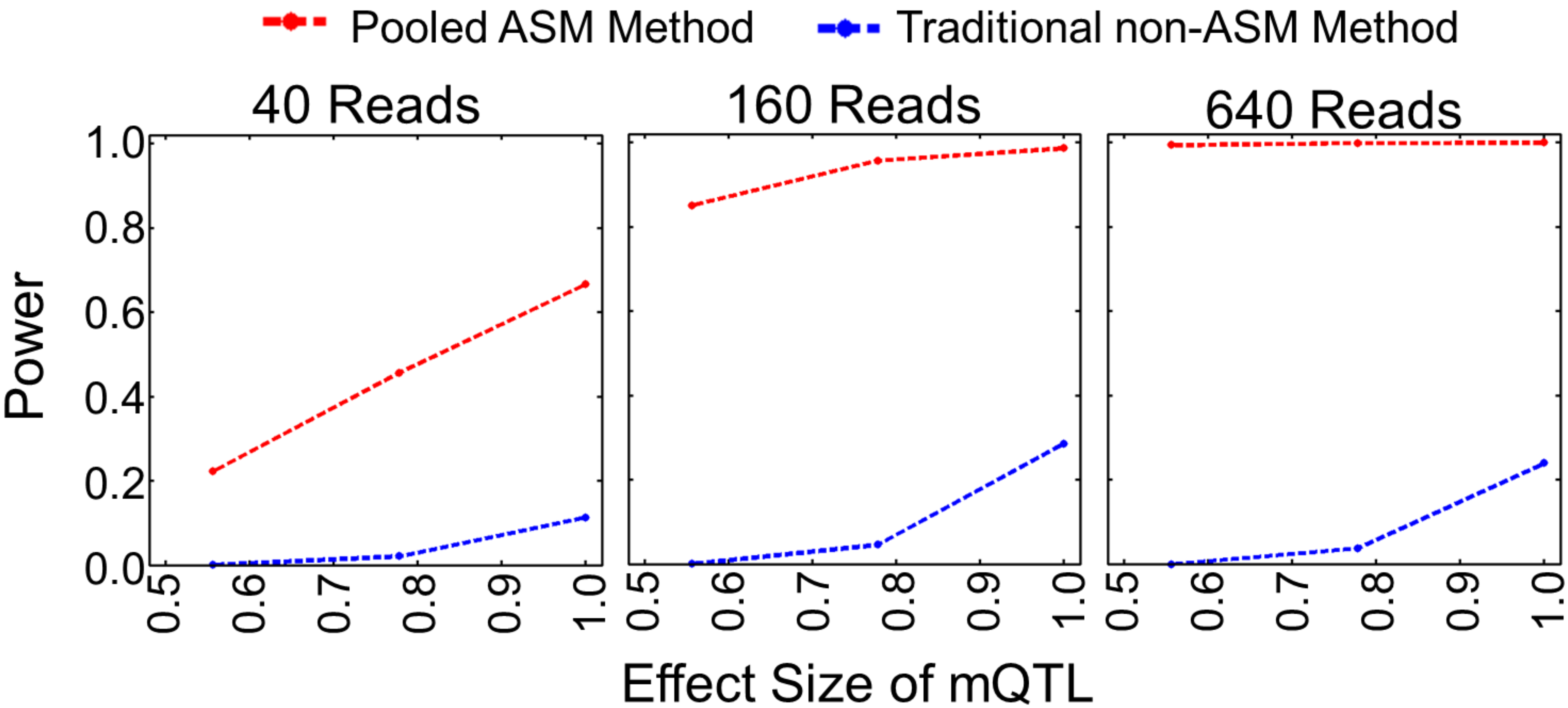

Supplemental Figure 8

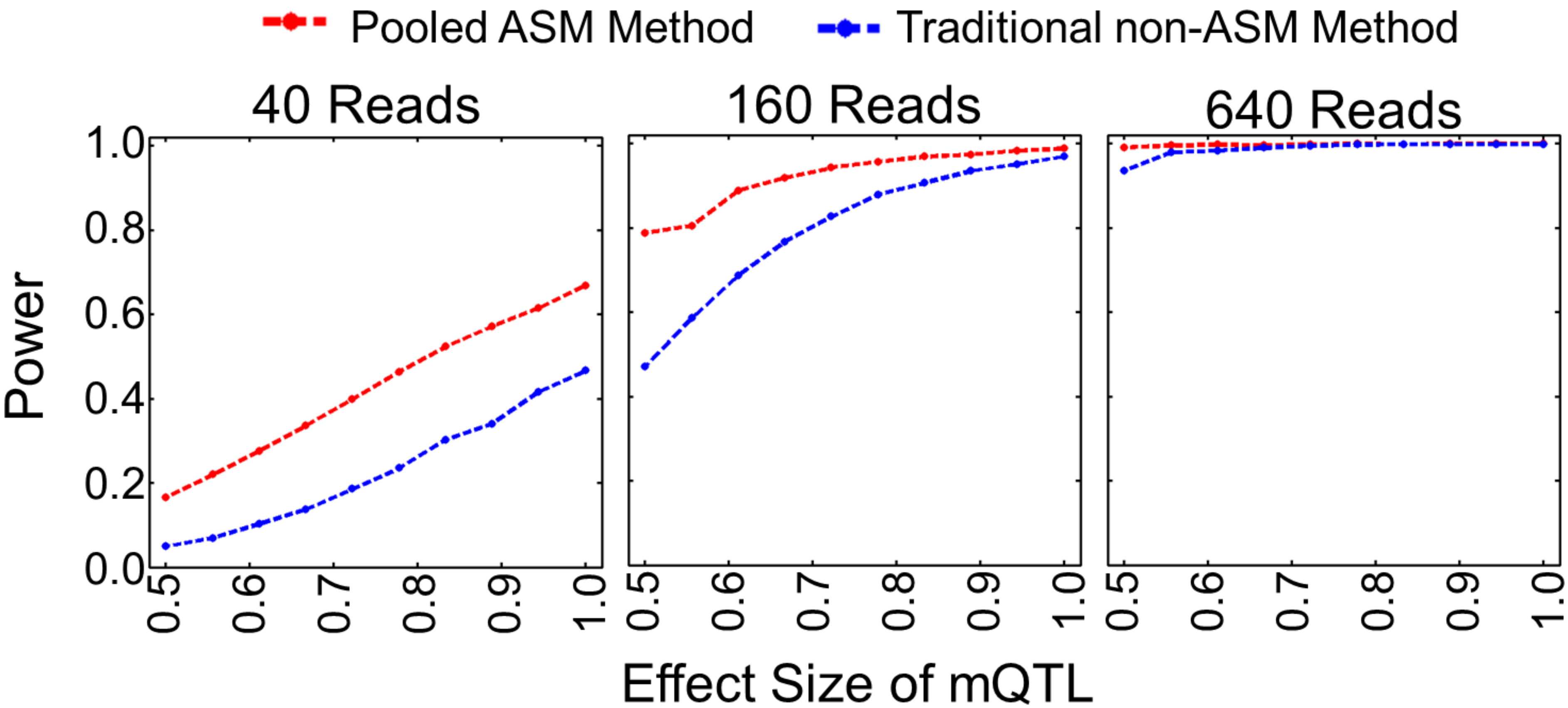

Supplemental Figure 9

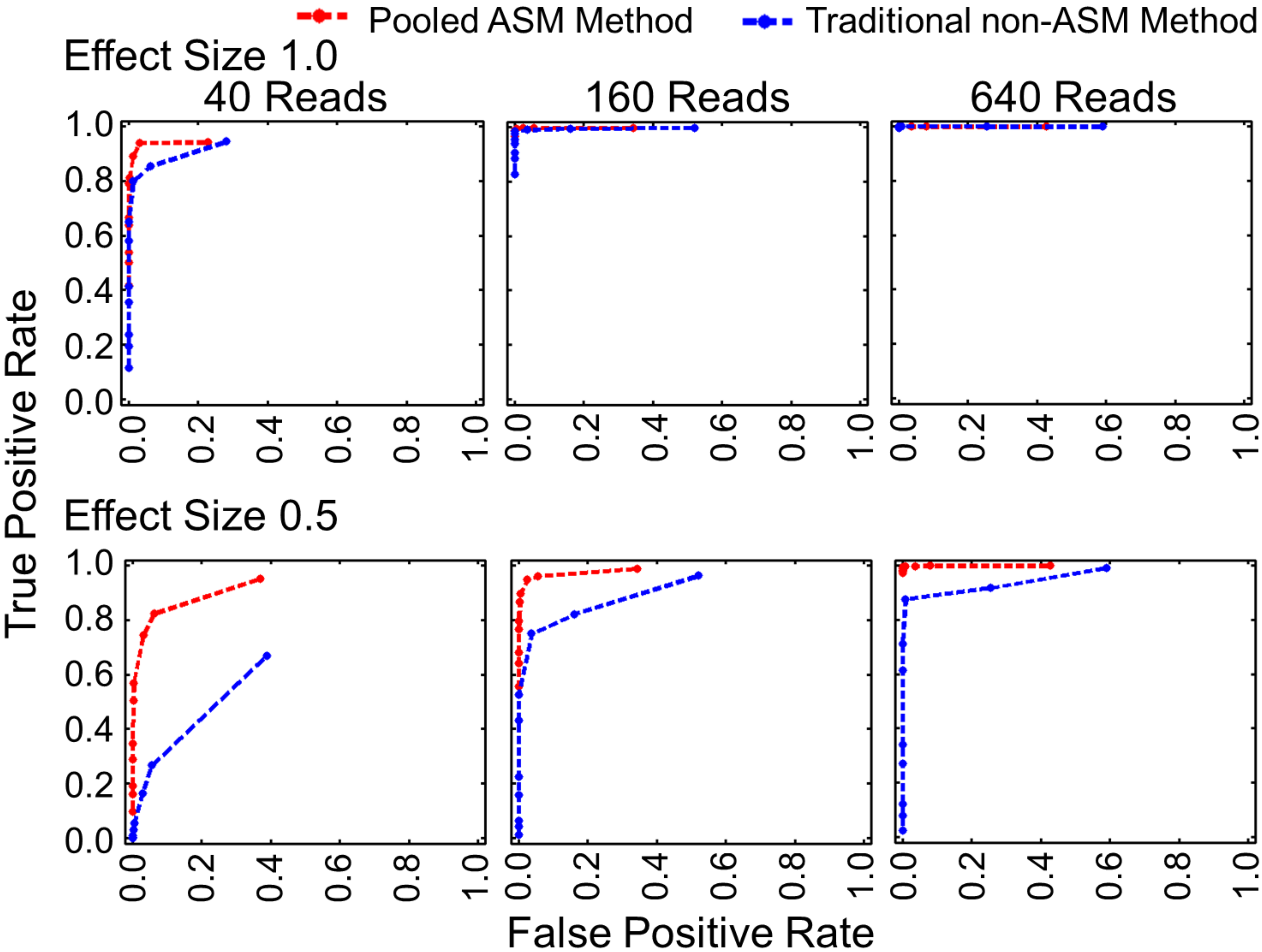

Supplemental Figure 10

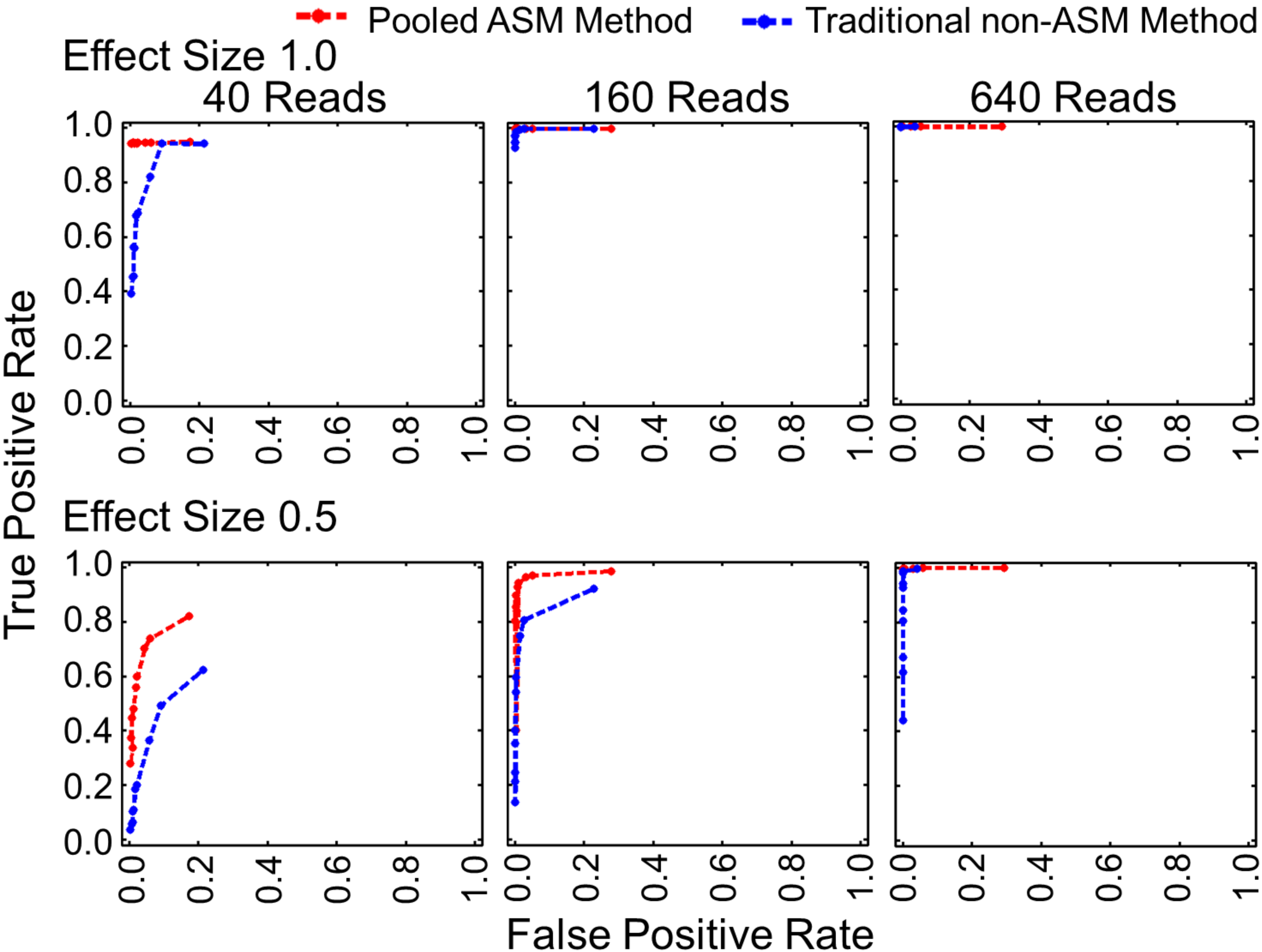

Supplemental Figure 11

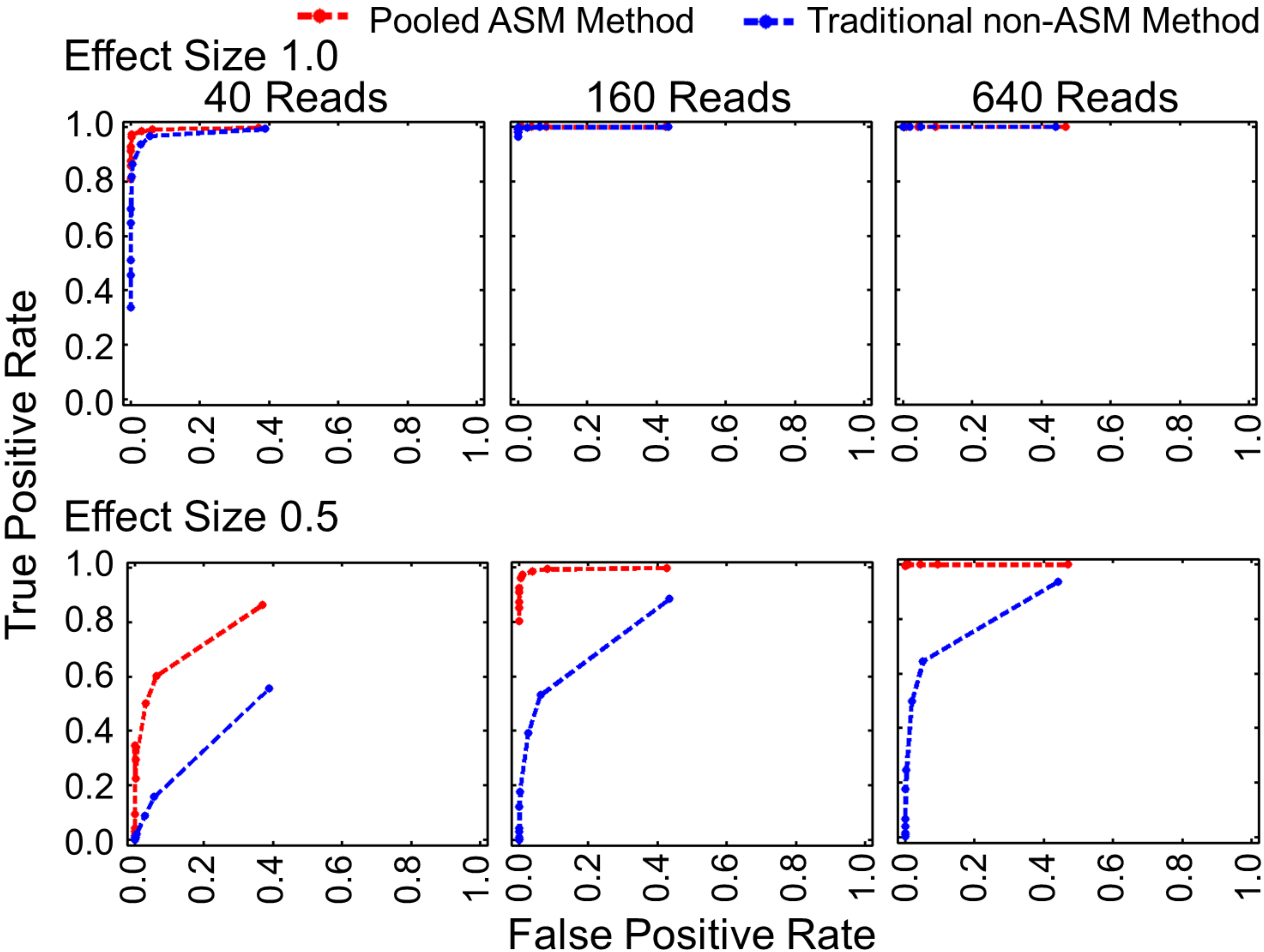

Supplemental Figure 12

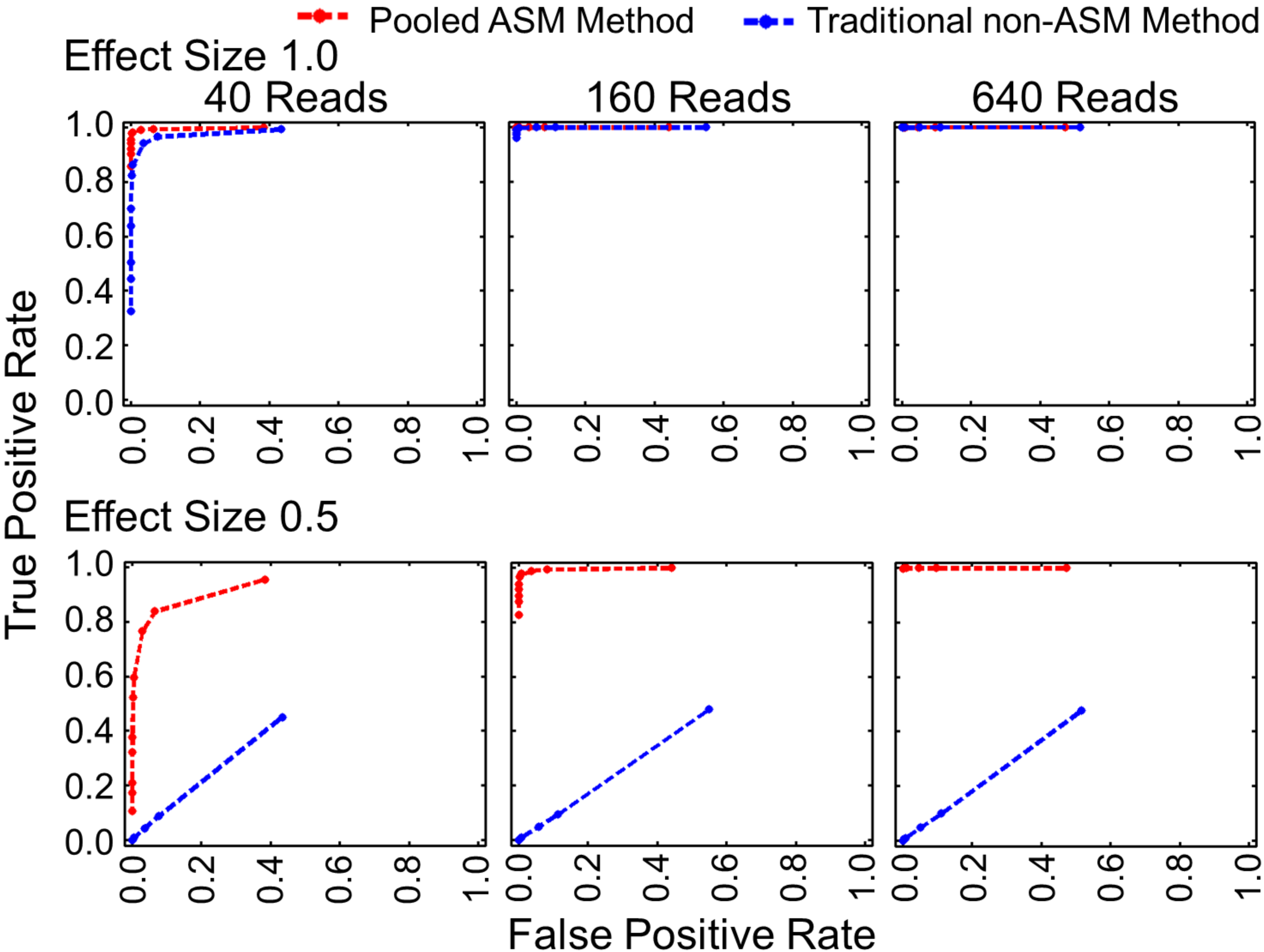

Supplemental Figure 13

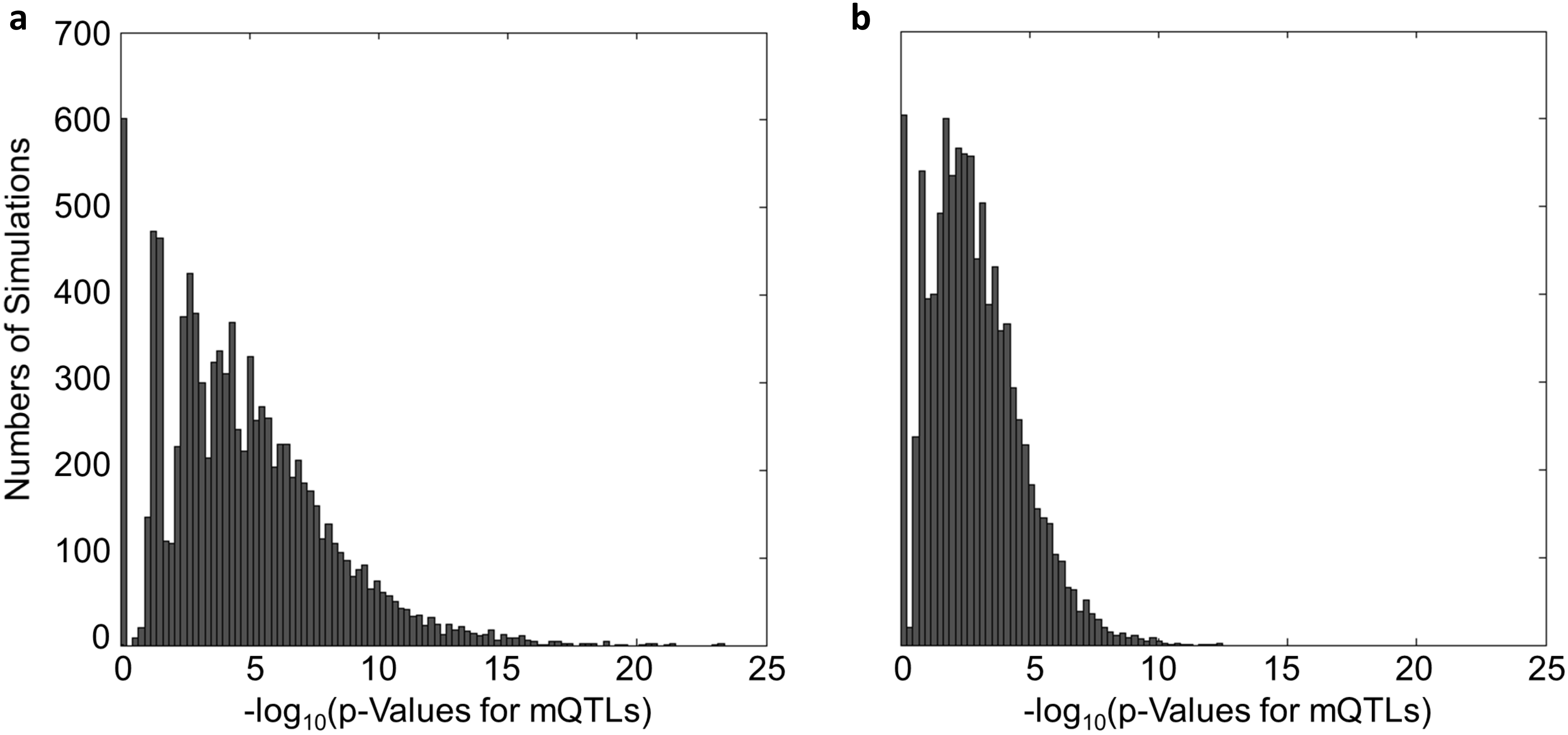

Supplemental Figure 14

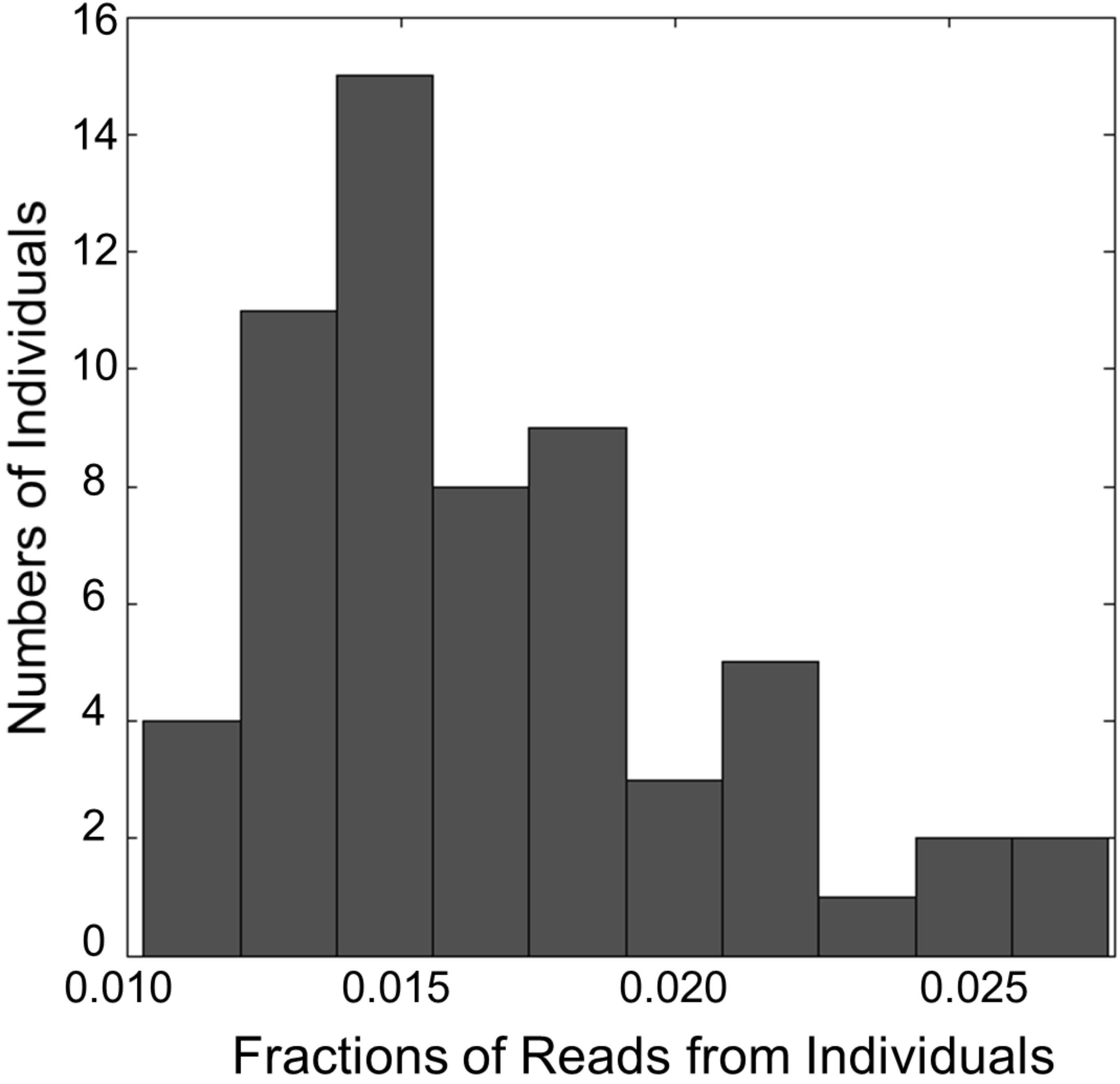

Supplemental Figure 15

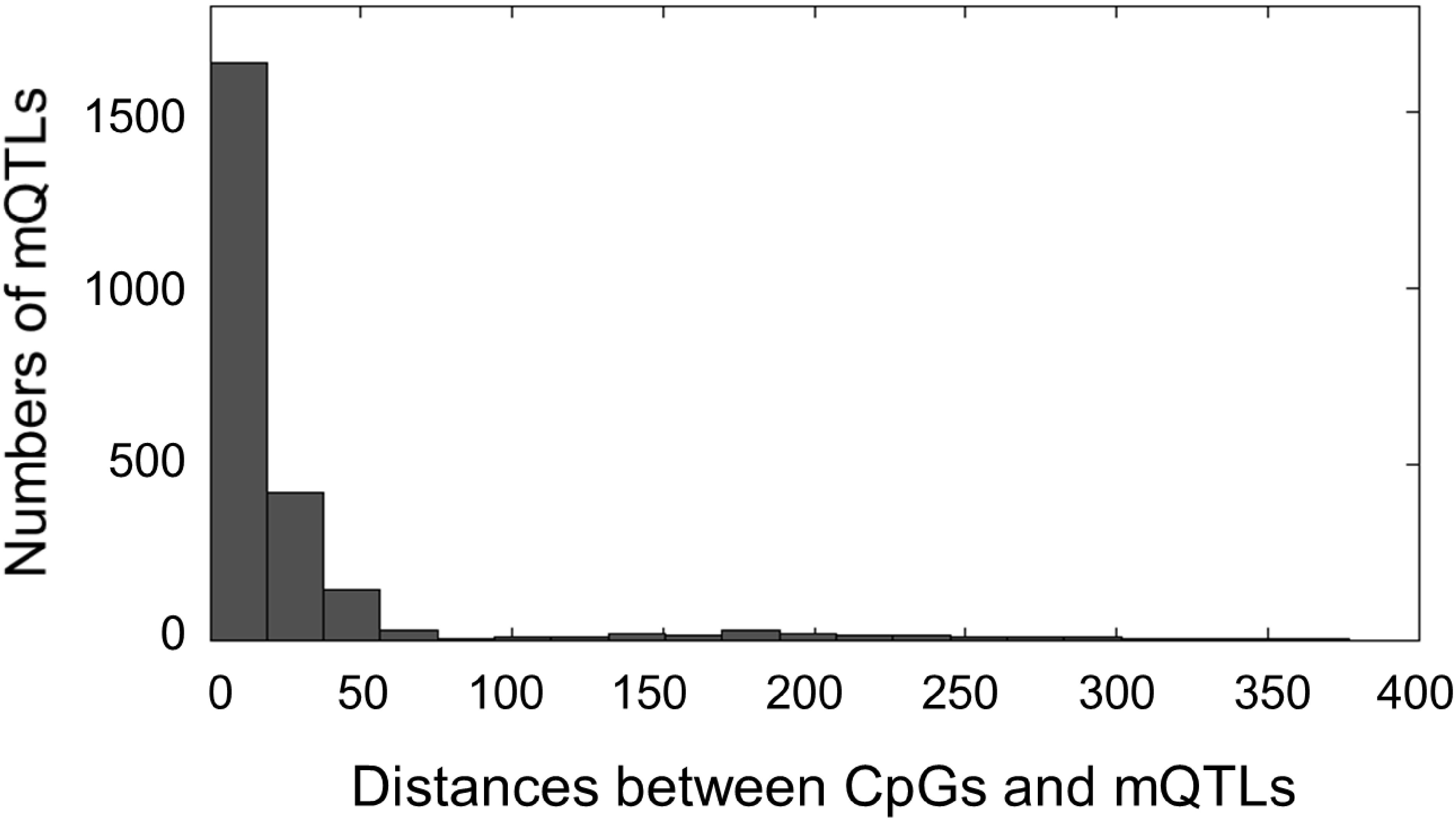

Supplemental Figure 16

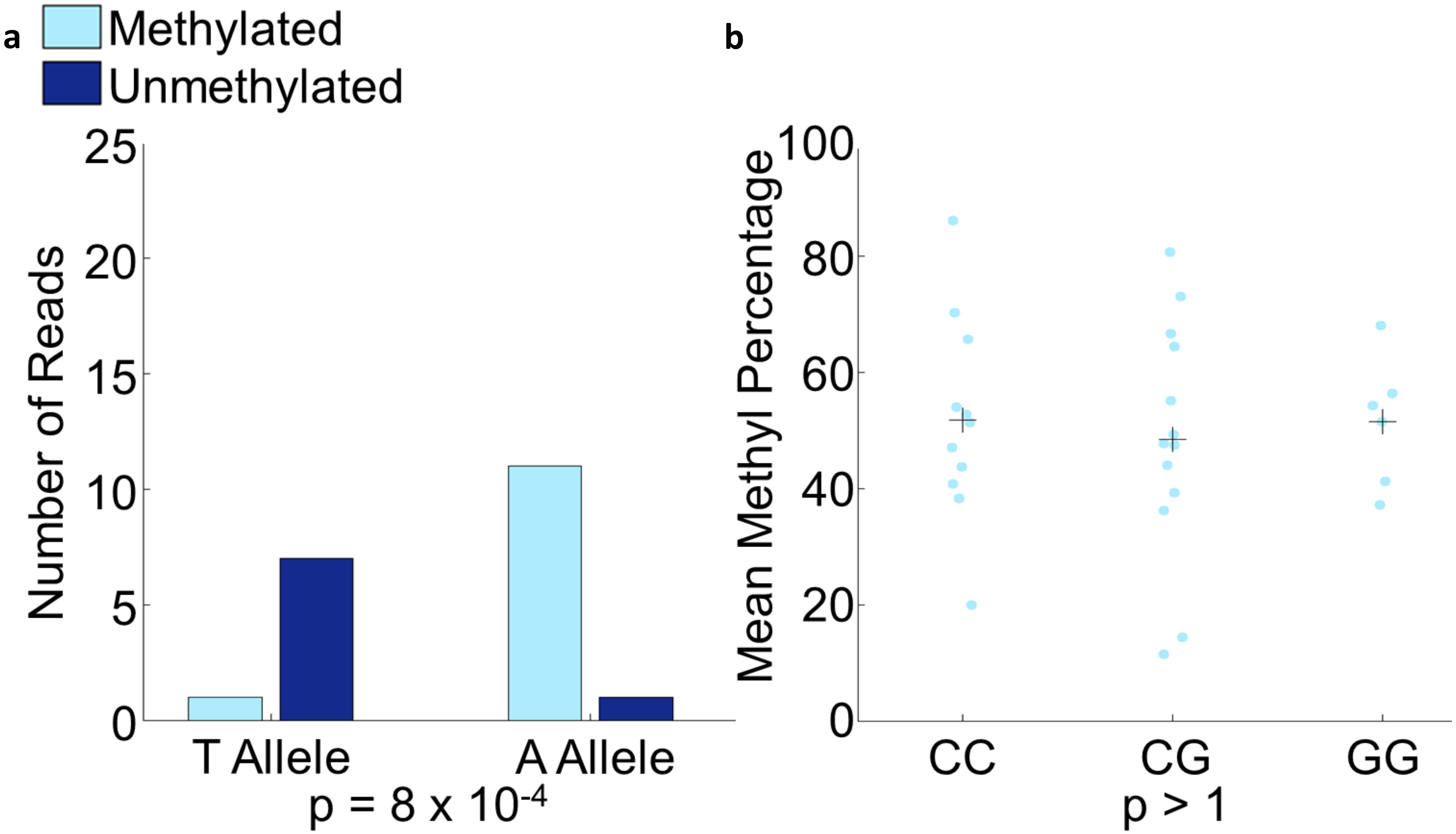

Supplemental Figure 17

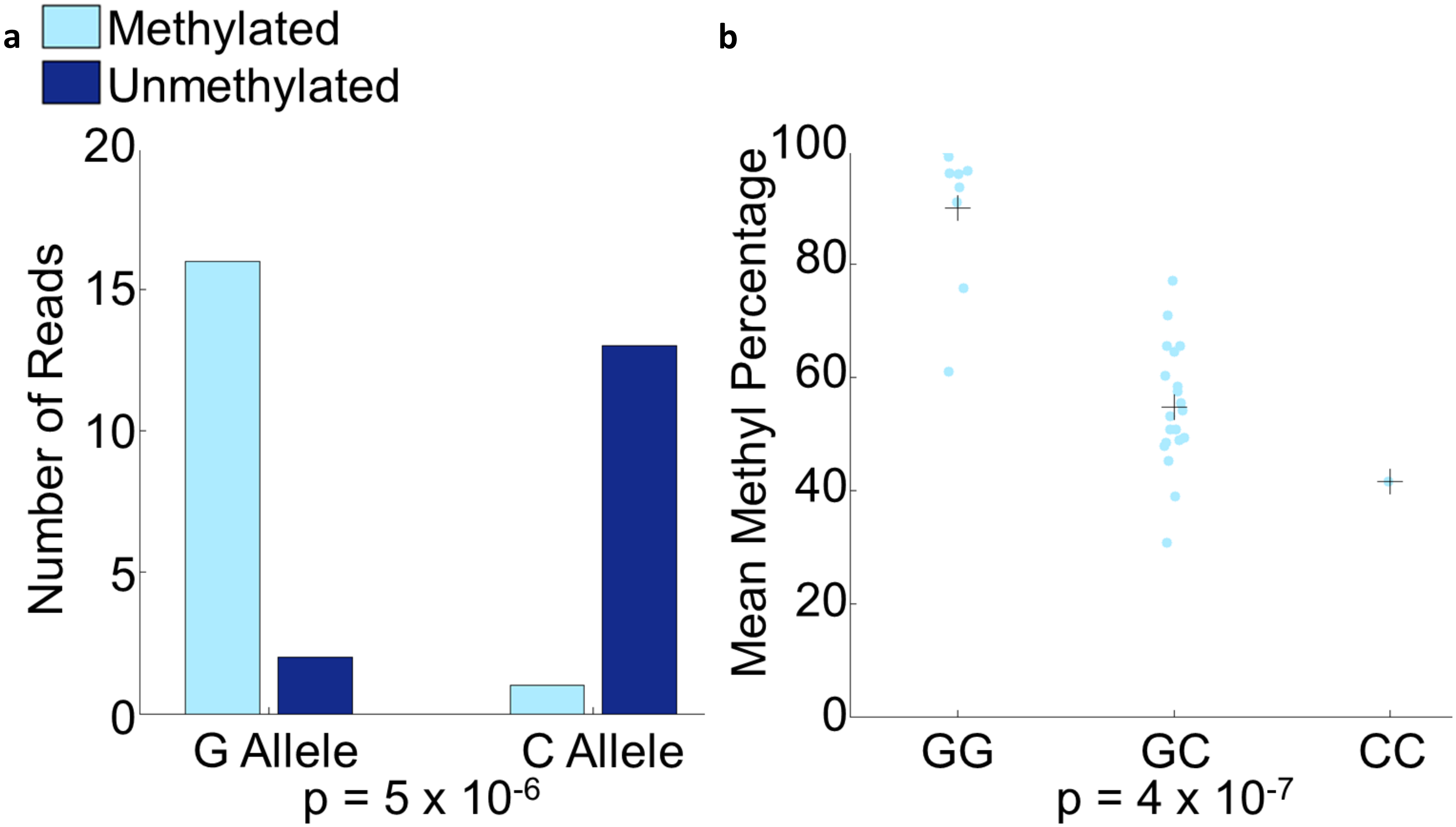

Supplemental Figure 18

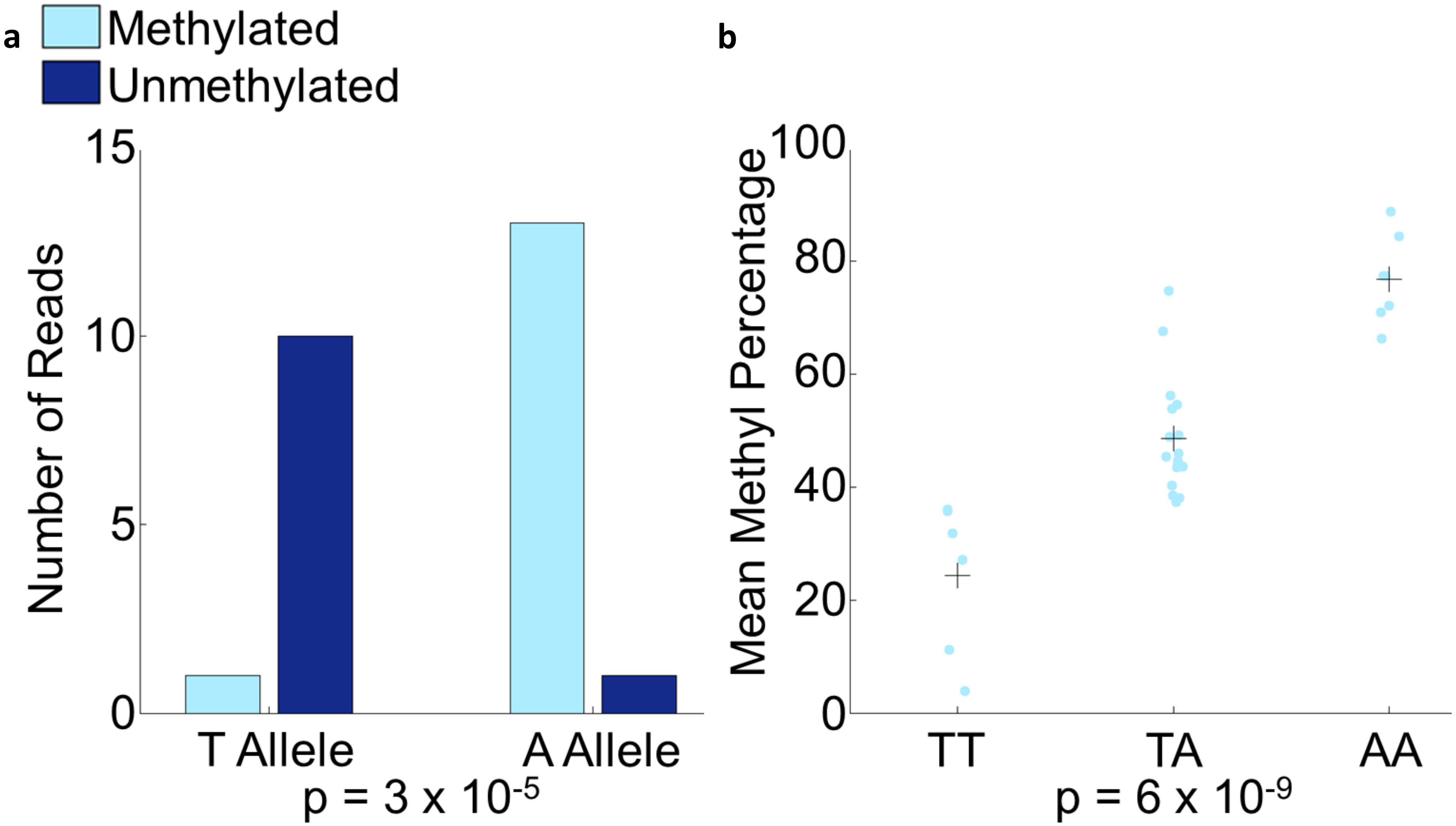

Supplemental Figure 19

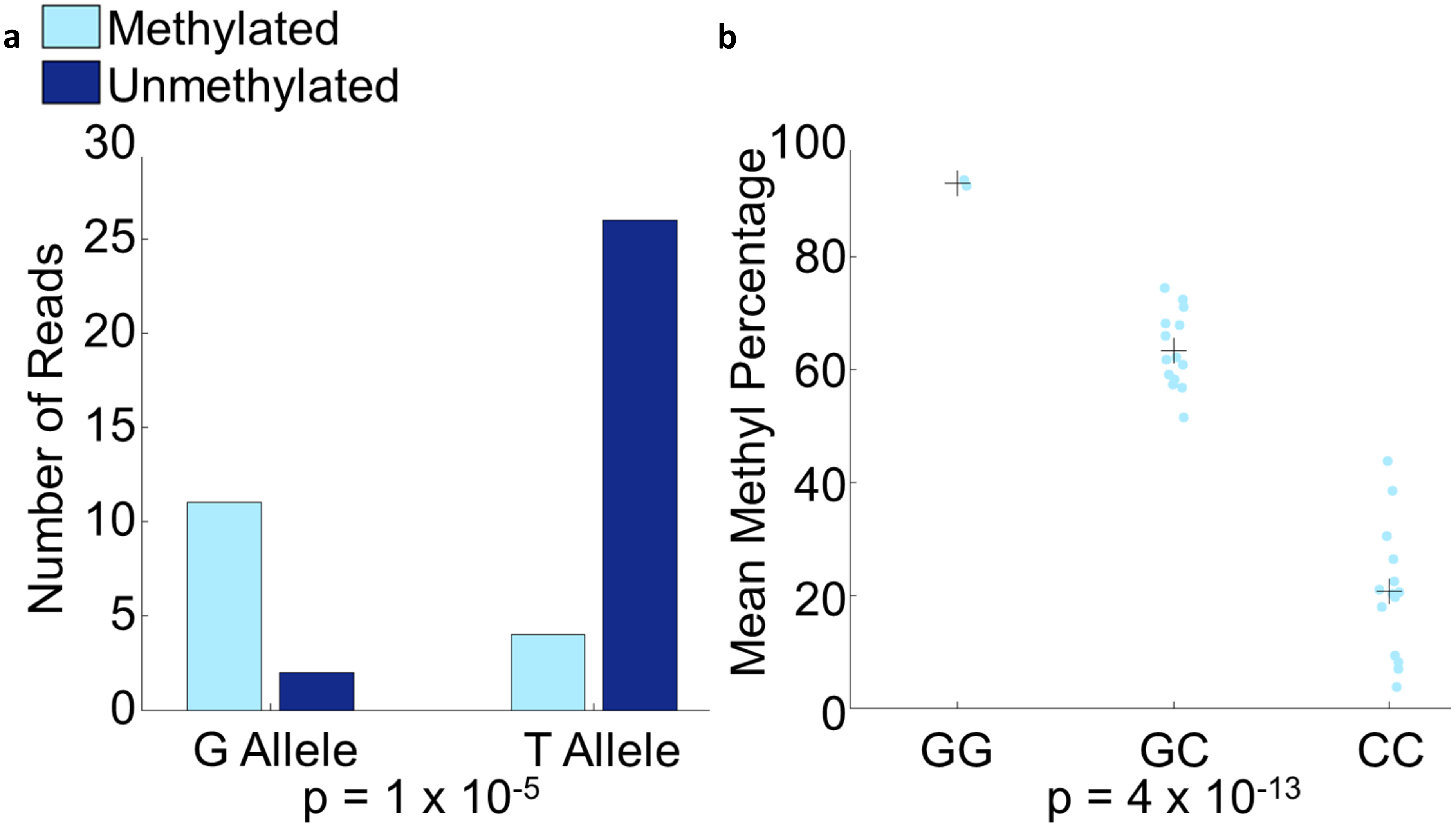

Supplemental Figure 20

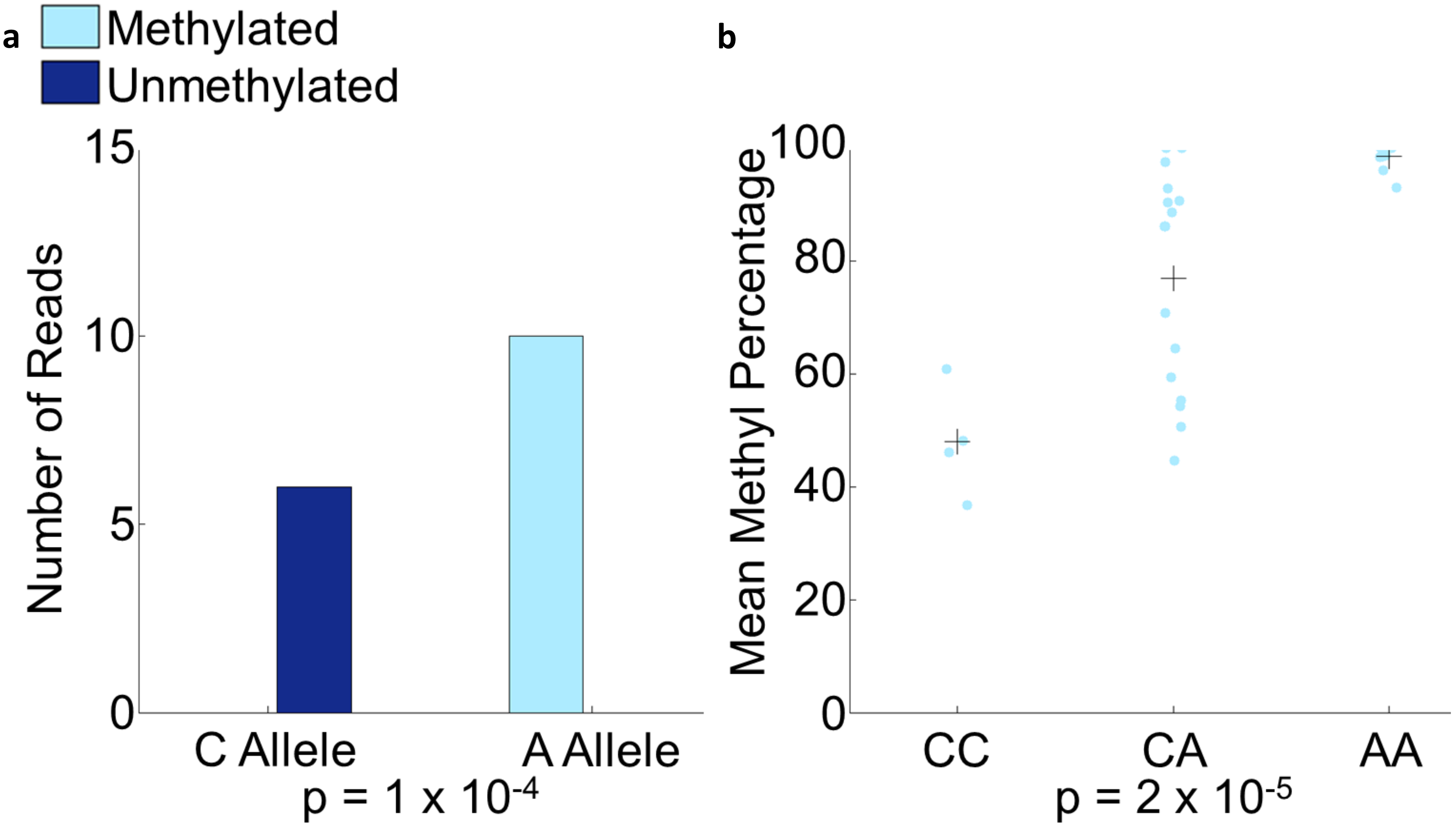

Supplemental Figure 21

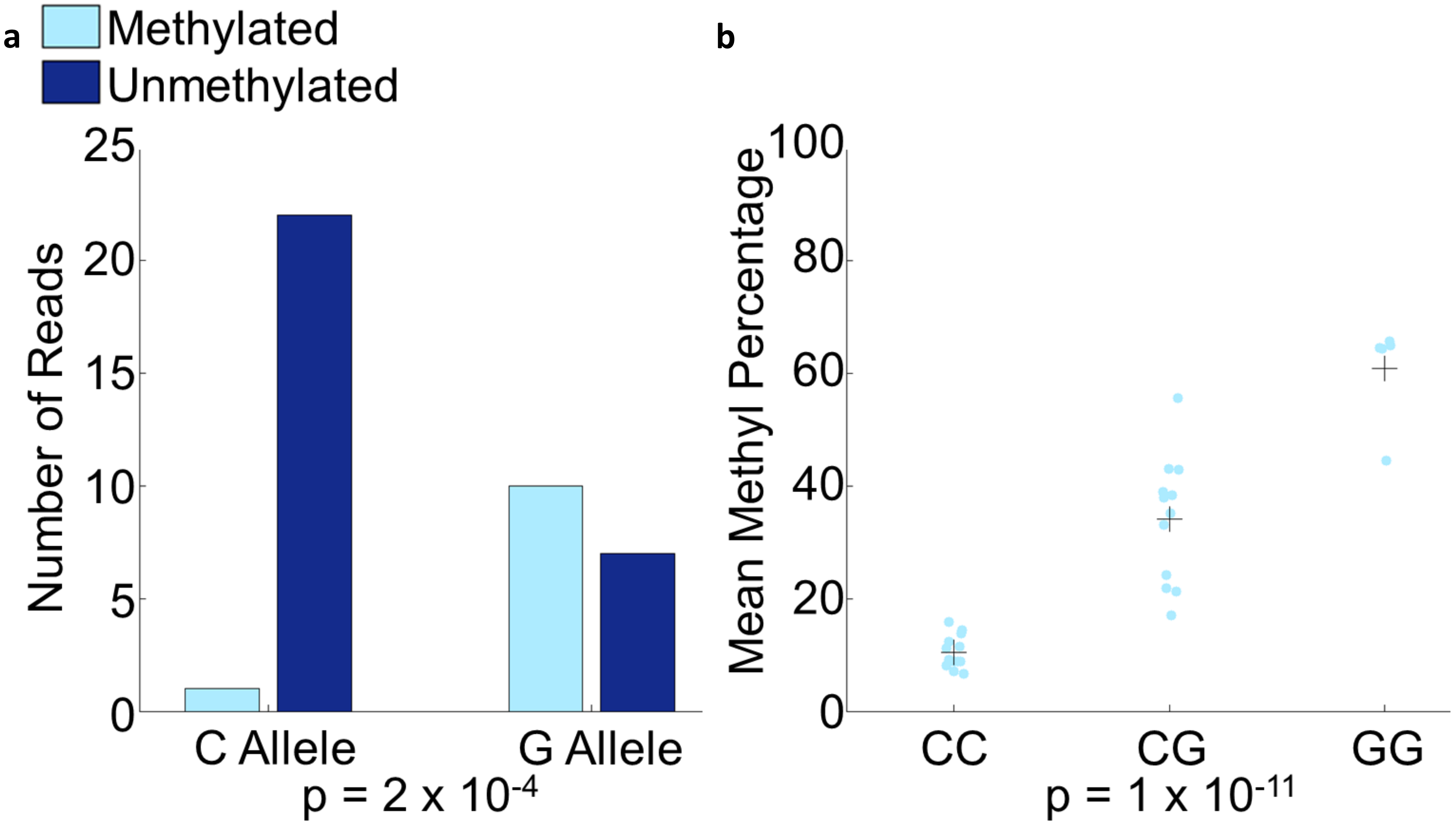

Supplemental Figure 22

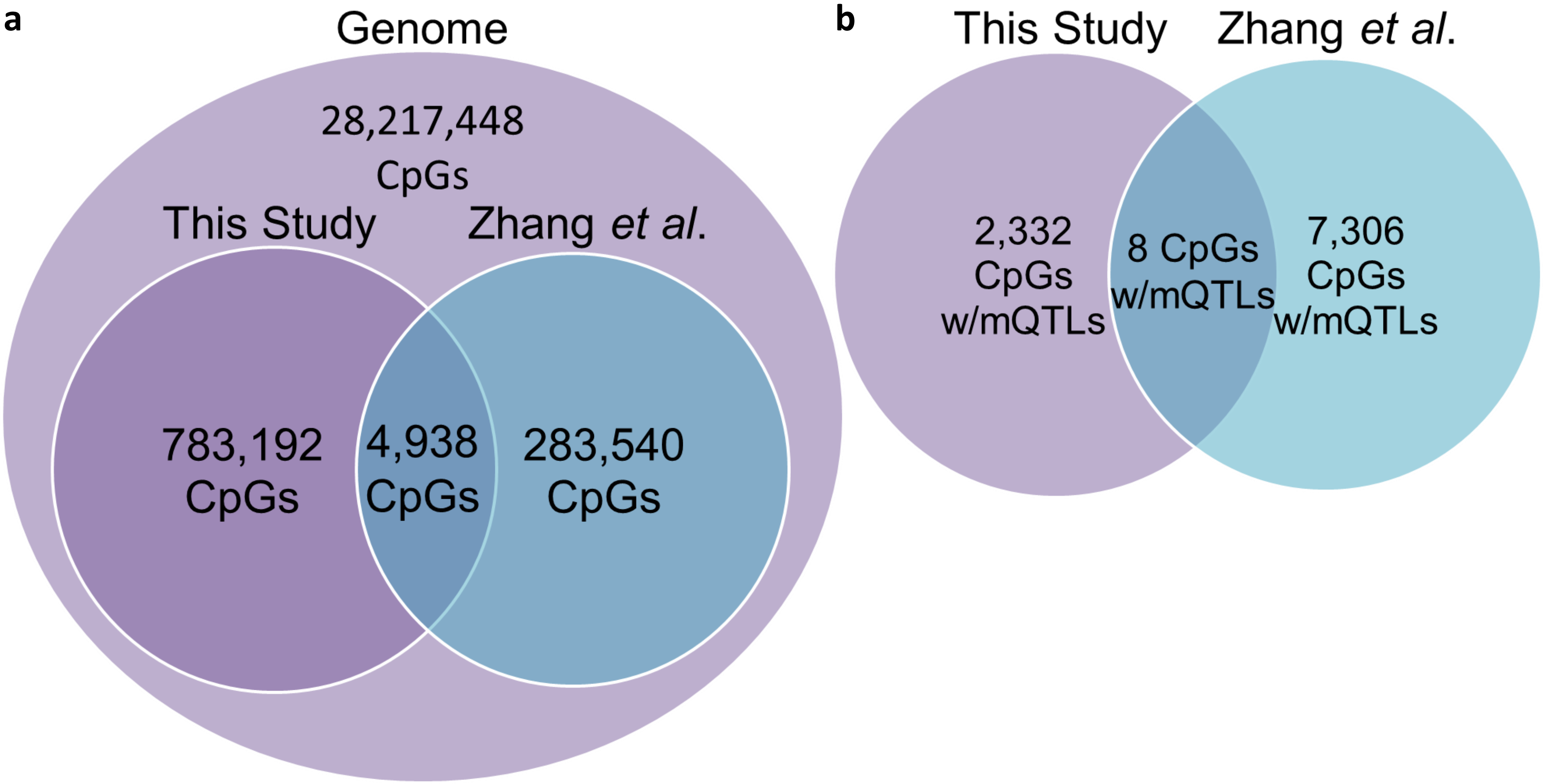

Supplemental Figure 23

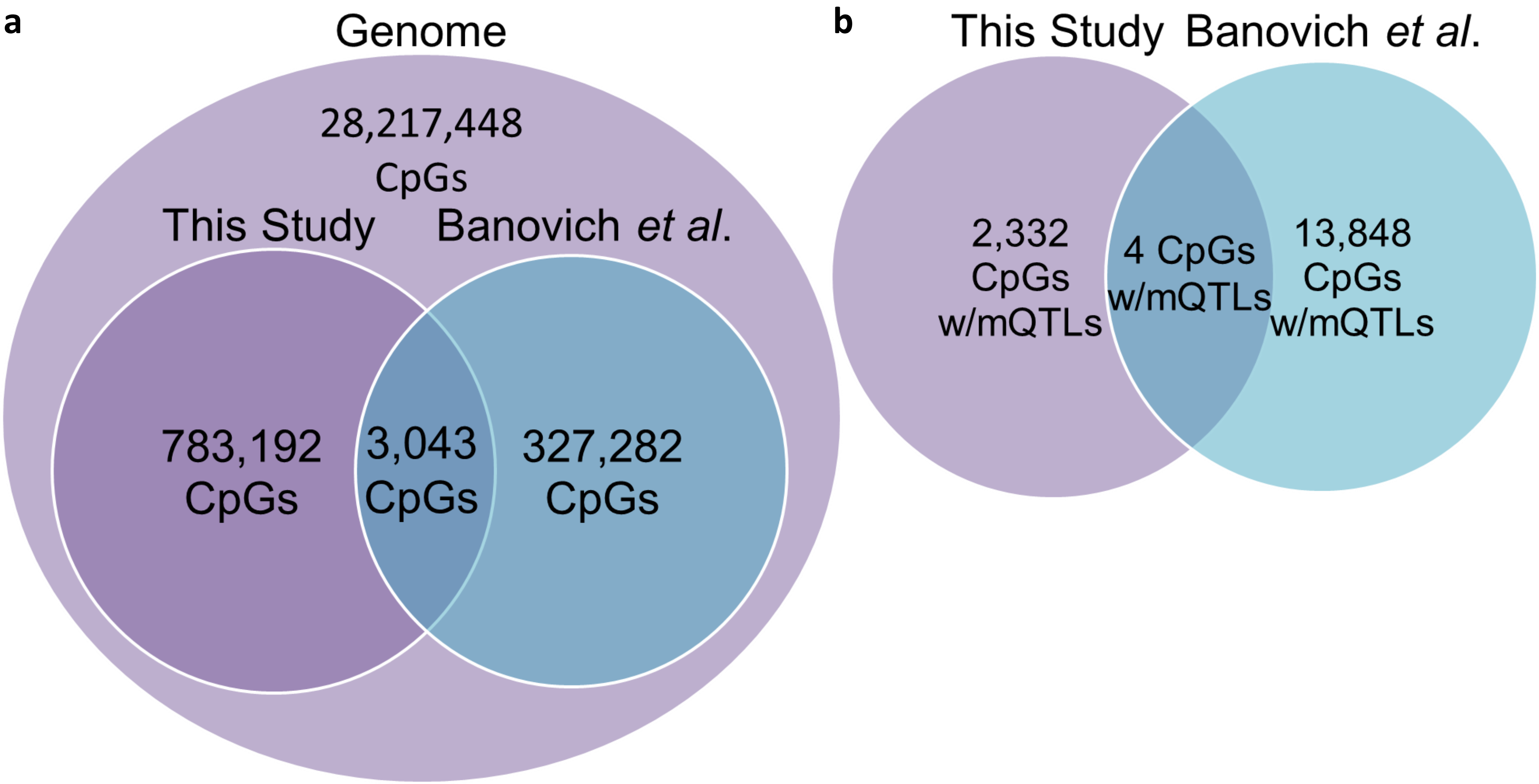

Supplemental Figure 24

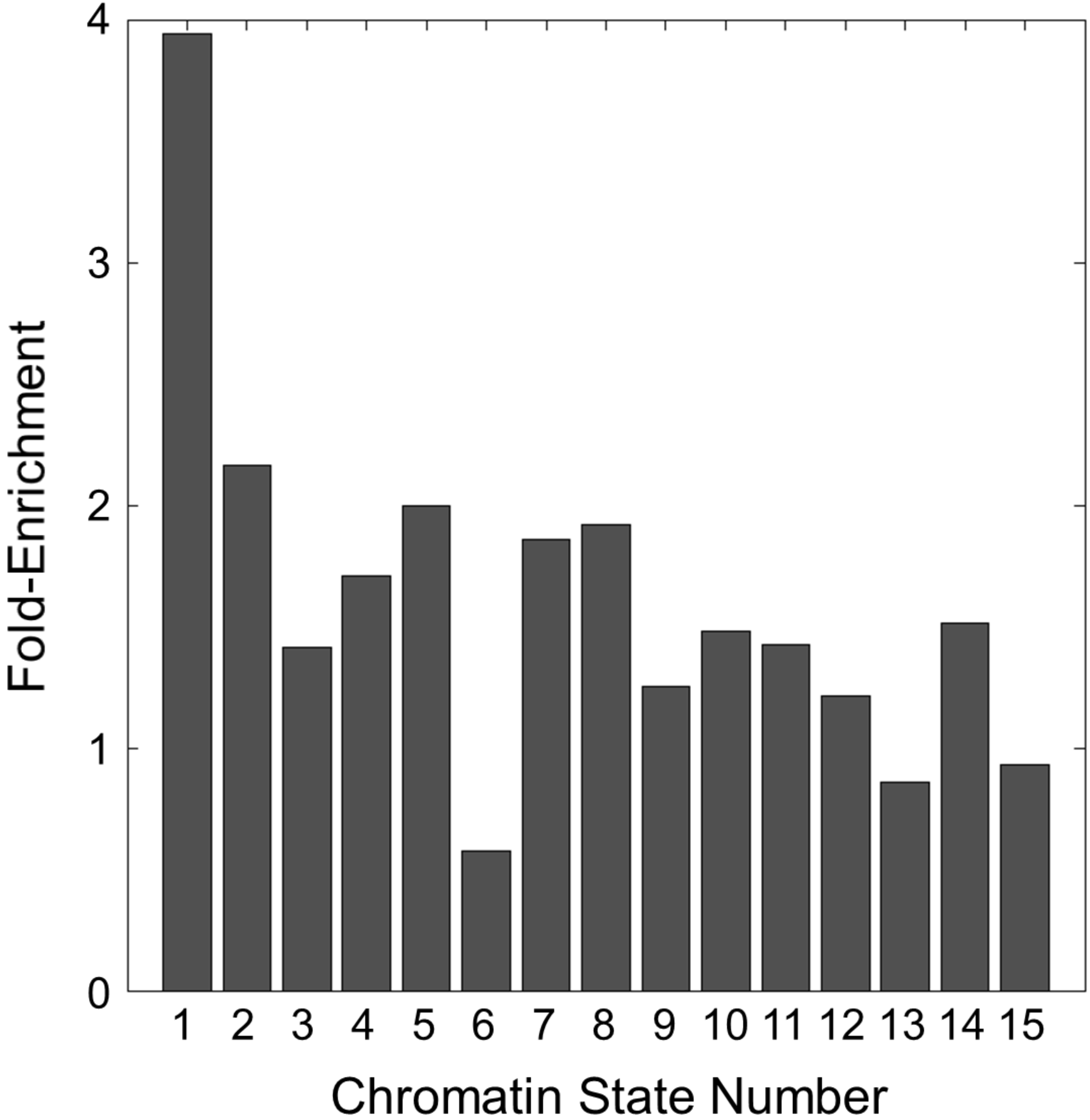

Supplemental Figure 25

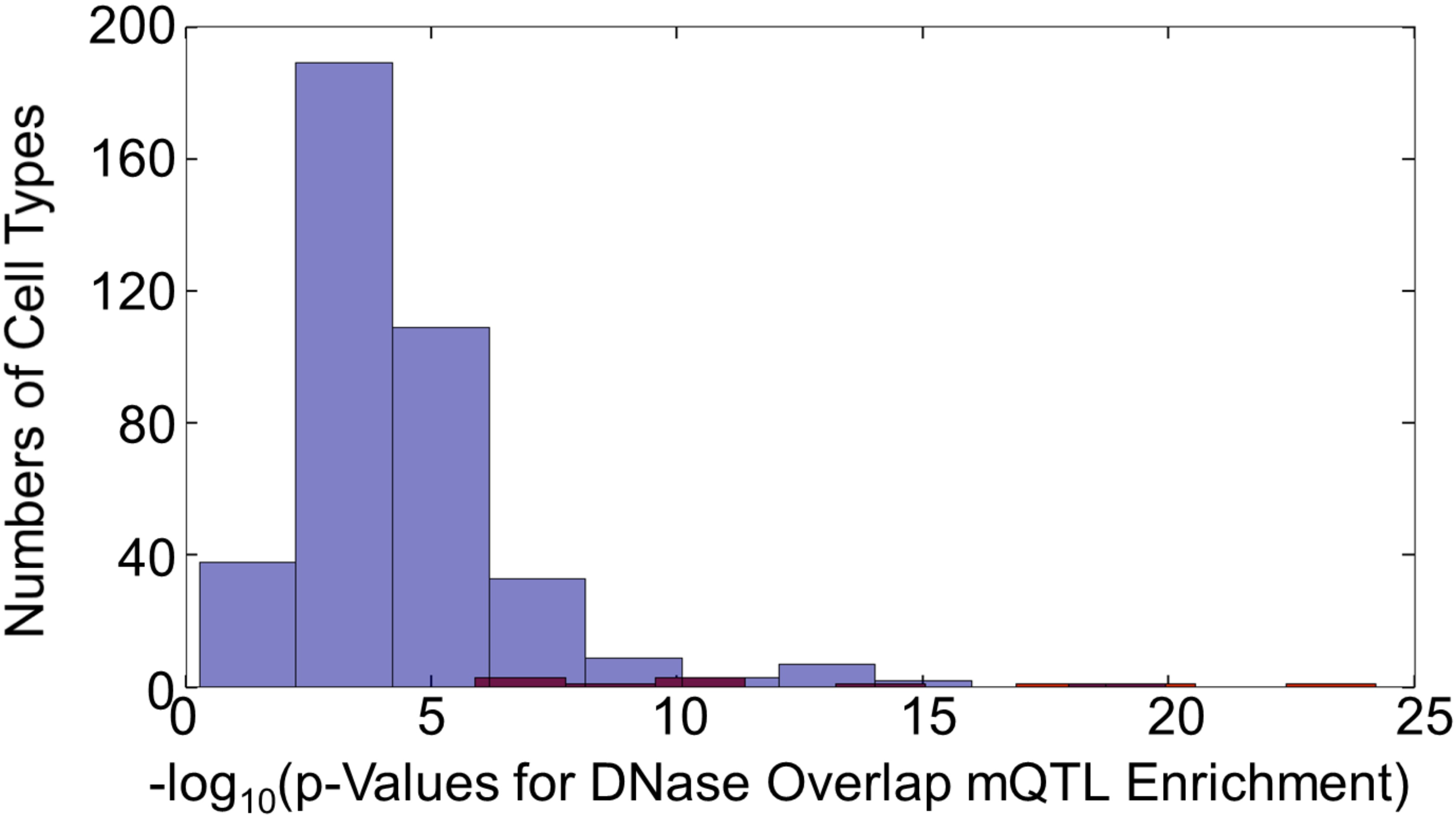

Supplemental Figure 26

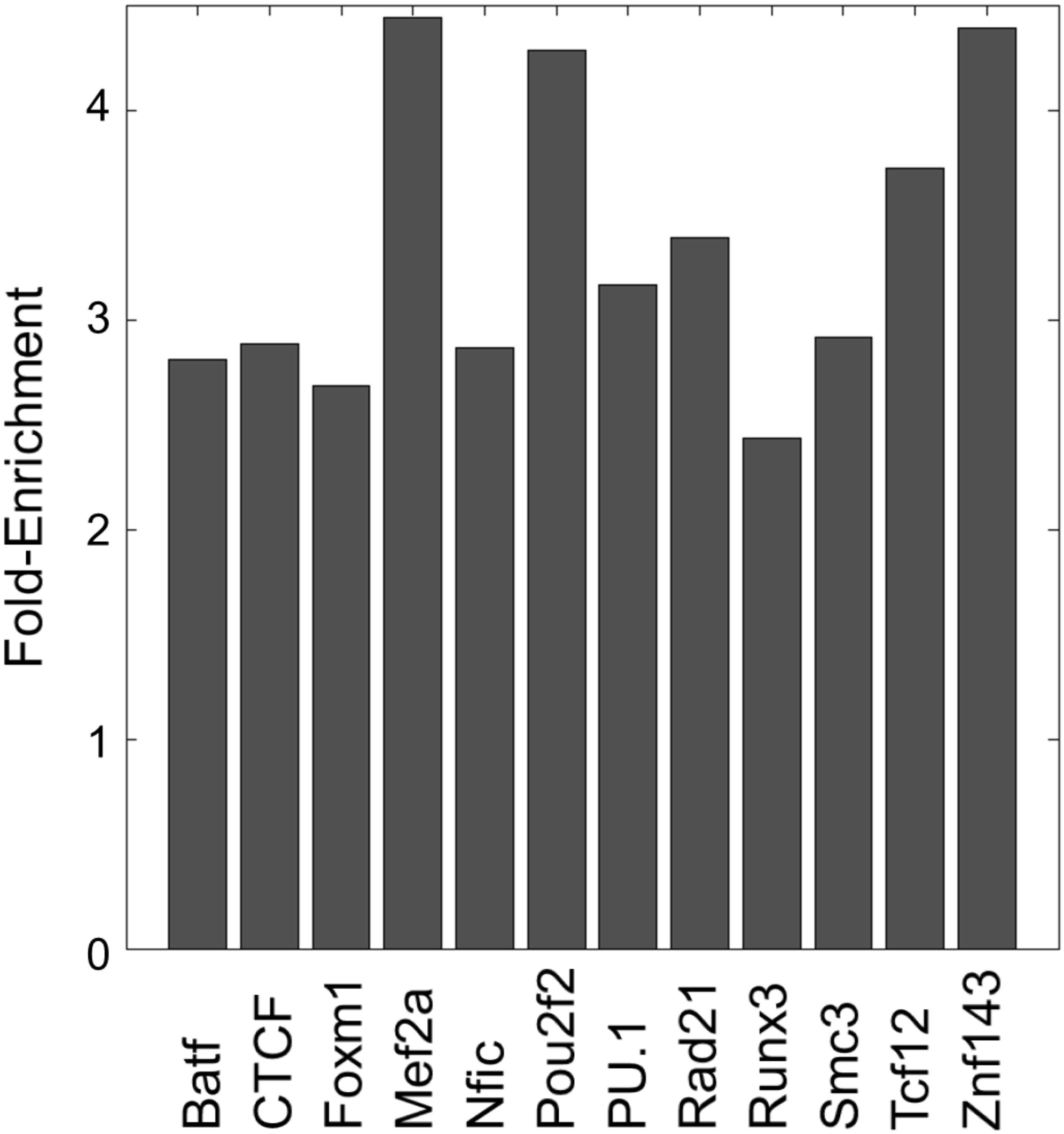

Supplemental Figure 27

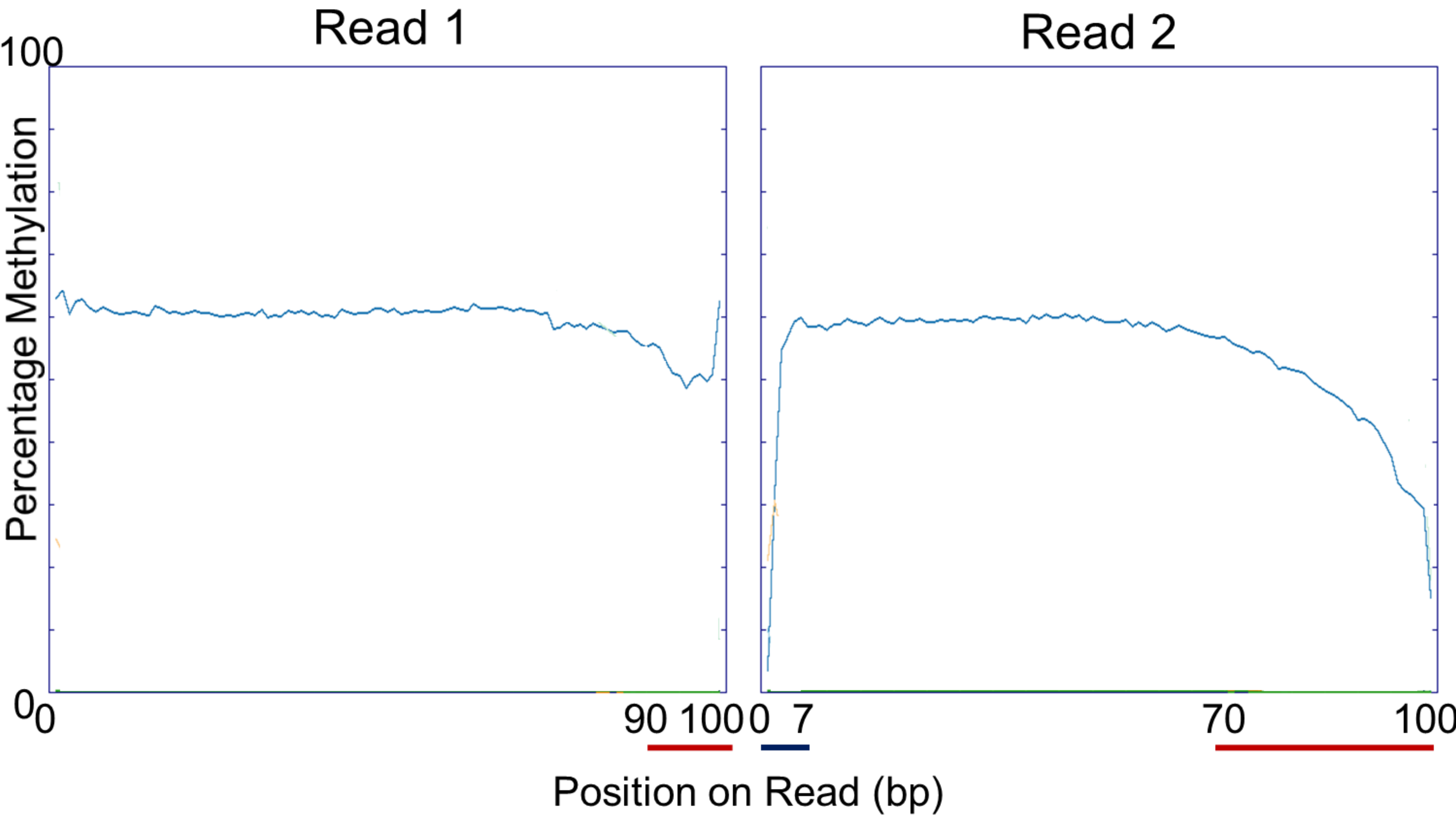

Supplemental Figure 28

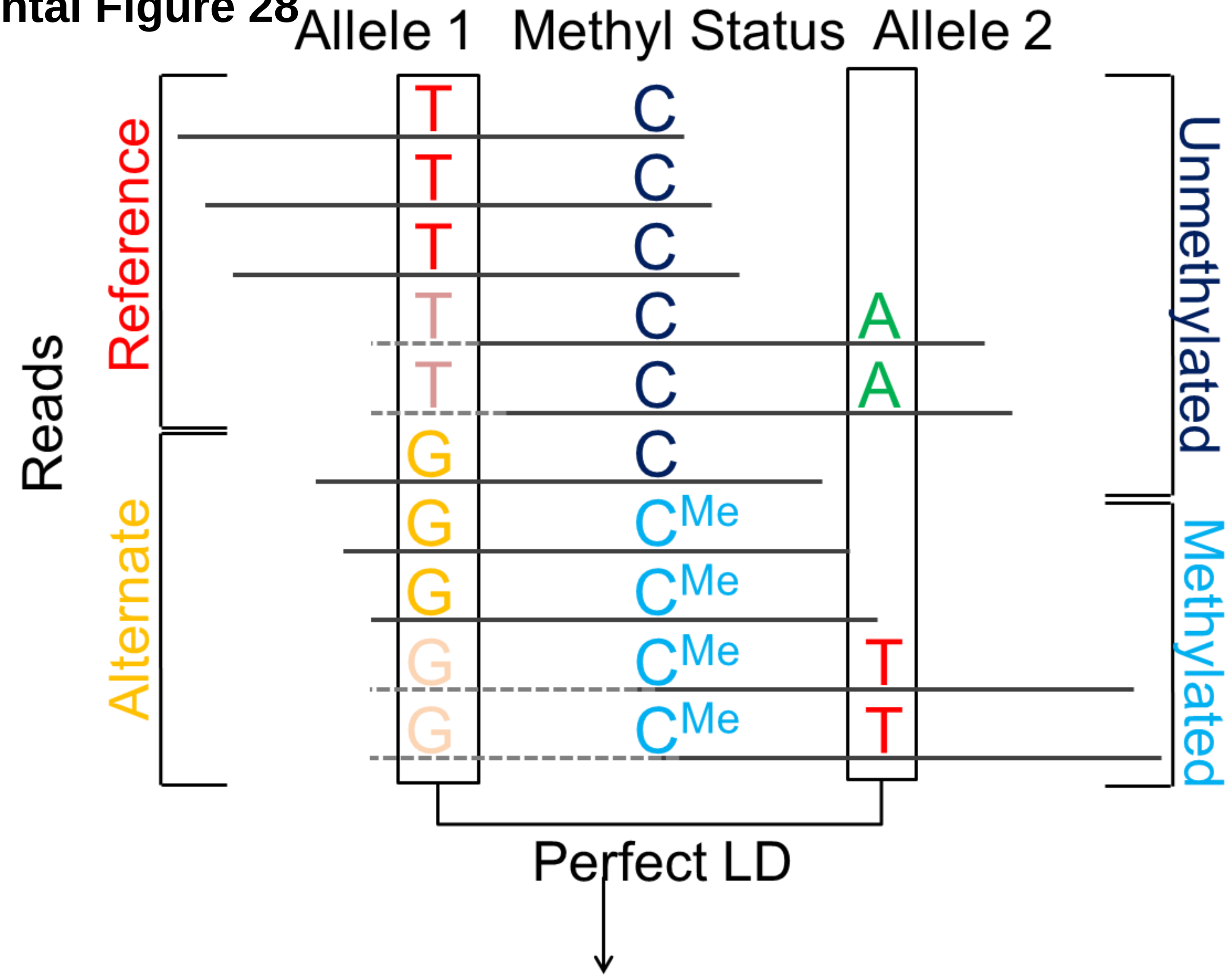

	Unmethyl	Methyl
Ref Allele (T)	5	0
Alt Allele (G)	1	4

Histone modification/ transcription factor	**Number of mQTLs in GM12878 region/peak**	**p-value for mQTL enrichment**
H2Az	51	1.13×10^{-1}
H3K4me1	92	> 1
H3K4me2	90	> 1
H3K4me3	41	> 1
H3K27ac	71	4.04×10^{-1}
H3K27me3	3	> 1
H3K36me3	19	> 1
H3K79me2	44	> 1
H3K9ac	34	> 1
H3K9me3	13	> 1
H4K20me1	2	> 1
Atf2	15	2.71×10^{-1}
Atf3	0	> 1
Batf	16	**2.55×10^{-2}**
Bcl11a	8	7.32×10^{-1}
Bcl3	5	> 1
Bclaf1	0	> 1
Bhlhe40	6	> 1
Brca1	0	> 1
Cebpb	3	> 1
c-Fos	0	> 1
Chd1	1	> 1
Chd2	5	> 1
c-Myc	0	> 1
CoREST	0	> 1
CTCF	31	**2.93×10^{-5}**
E2f4	0	> 1
Ebf1	10	> 1
Egr1	3	> 1
Elf1	6	> 1
Elk1	1	> 1
Ets1	1	> 1
Ezh2	0	> 1
Foxm1	16	**4.15×10^{-2}**
Gabp	1	> 1
Gcn5	0	> 1
Ikzf1	3	> 1
Irf3	0	> 1
Irf4	9	4.46×10^{-1}
JunD	0	> 1
Max	3	> 1
Maz	4	> 1
Mef2a	10	**1.06×10^{-2}**
Mef2c	6	1.23×10^{-1}

Mta3	5	> 1
Mxi1	1	> 1
Nfat	8	> 1
Nfe2	0	> 1
Nfic	27	**1.82 x 10^{-4}**
Nfkb	7	> 1
Nfya	0	> 1
Nfyb	3	> 1
Nrf1	0	> 1
NRSF	2	> 1
p300	7	> 1
Pax5C	10	> 1
Pax5N	11	1.90 x 10^{-1}
Pbx3	0	> 1
Pml	6	> 1
Pol2, 4h	9	> 1
Pol2	9	> 1
Pol2-S2	1	> 1
Pol3	0	> 1
Pou2f2	14	**7.56 x 10^{-4}**
PU.1	21	**1.09 x 10^{-3}**
Rad21	19	**5.87 x 10^{-4}**
Rfx5	0	> 1
Runx3	37	**6.65 x 10^{-5}**
Rxra	0	> 1
Sin3a	3	> 1
Six5	2	> 1
Smc3	18	**7.11 x 10^{-3}**
Sp1	6	> 1
Spt20	71	> 1
Srf	4	> 1
Stat1	1	> 1
Stat3	1	> 1
Stat5	7	> 1
Taf1	2	> 1
Tblr1	4	> 1
Tbp	4	> 1
Tcf12	11	**2.30 x 10^{-2}**
Tcf3	9	2.81 x 10^{-1}
Tr4	1	> 1
Usf1	2	> 1
Usf2	6	> 1
Whip	8	> 1
Yy1	9	> 1
Zbtb33	1	> 1
Zeb1	1	> 1

Znf143	12	**2.57×10^{-3}**
Znf274	0	> 1
Zzz3	0	> 1

Supplemental Table 1: Enrichment of mQTLs in GM12878 regions/peaks

All p-values are Bonferroni-corrected. GM12878 peaks for twelve TFs are enriched for mQTLs; these TFs are shown in bold. The sites for all of these TFs contain at least ten mQTLs.

Molecular QTL	**Number of mQTL intersections**	**Number of mQTL intersections, including variants in perfect LD**	**Number of mQTL intersections, including variants in r^2 ≥ 0.8 LD**
eQTL from Pickrell *et al*.	0	3	5
sQTL from Pickrell *et al*.	0	0	0
Exon-level eQTL from GEUVADIS Consortium	28	28	32
Gene-level eQTL from GEUVADIS Consortium	5	5	9
dsQTL from Degner *et al*.	34	48	74
CTCF-binding-QTL from Ding *et al*.	15	18	28

Supplemental Table 2: Numbers of mQTL intersections with other molecular QTL datasets

Other QTL data-sets were expanded to incorporate variants at different levels of LD in 1000 Genomes. dsQTLs were from the combined list of dsQTLs with both distance cutoffs used in Degner *et al*.

Molecular QTL	**Fold enrichment of mQTL intersections**	**Fold enrichment of mQTL intersections, including variants in perfect LD**	**Fold enrichment of mQTL intersections, including variants in r^2 ≥ 0.8 LD**
eQTL from Pickrell *et al*.	N/A	3.16	1.95
sQTL from Pickrell *et al*.	N/A	0.00	0.00
Exon-level eQTL from GEUVADIS Consortium	1.91	1.78	1.68
Gene-level eQTL from GEUVADIS Consortium	1.58	1.46	2.22
dsQTL from Degner *et al*.	10.75	7.27	4.98
CTCF-binding-QTL from Ding *et al*.	2.70	2.48	2.41

Supplemental Table 3: Fold enrichments for mQTL intersections with other molecular QTL datasets

Fold enrichment is (number of mQTL intersections)/(expected number of mQTL intersections). Other QTL datasets were expanded to incorporate variants at different levels of LD in 1000 Genomes. dsQTLs were from the combined list of dsQTLs with both distance cutoffs used in Degner *et al*. N/A indicates that no molecular QTLs were tested for having mQTLs.

mQTL rsID	CpG position	GWAS SNP rsID	LD (r^2) between mQTL and GWAS SNP	GWAS trait	GWAS paper PMID(s)
rs10888935	chr1:56060953	rs10888935	mQTL is GWAS SNP	Inflammatory biomarkers	22228203
rs10797916	chr1:183838064	rs4651156	1.00	Response to antidepressants	20360315
rs10737680	chr1:196679457	rs10737680	mQTL is GWAS SNP	Age-related macular degeneration	23455636, 20385819
rs801736	chr11:65928440	rs564343	0.81	Obesity (early onset extreme)	23563609
rs9517668	chr13:99923789	rs7335046	0.80	Basal cell carcinoma	21700618
rs9806806	chr16:9916205	rs8058295	0.87	Autism spectrum disorder, attention deficit-hyperactivity disorder, bipolar disorder, major depressive disorder, and schizophrenia (combined)	23453885
rs617201	chr17:30893145	rs225212	0.84	Hypertension risk in short sleep duration	22322875
rs1113144	chr18:71774787	rs9945428	1.00	Venous thromboembolism	23509962
rs885252	chr2:39850639	rs7587205	0.96	Response to angiotensin II receptor blocker therapy (opposite direction w/ diuretic therapy)	22566498
rs16826873	chr2:198898223	rs1016883	0.80	Ulcerative colitis	23128233
rs4809455	chr20:61660749	rs6089829	0.90	Prostate cancer	22219177
rs4809456	chr20:61660870	rs6089829	0.86	Prostate cancer	22219177
rs2837821	chr21:42161839	rs2837828	1.00	Neutrophil count	21507922
rs1904394	chr3:2653208	rs4370013	0.86	Blood pressure	17903302
rs2673051	chr3:45732458	rs2742417	0.93	Response to antidepressant treatment	22041458
rs4859682	chr4:77410304	rs4859682	mQTL is GWAS SNP	Glomerular filtration rate	23535967
rs830885	chr5:52021828	rs830884	1.00	Response to platinum-based agents	22020760
rs2400797	chr5:101781191	rs1502844	0.92	Schizophrenia	19571808
rs7705033	chr5:122774795	rs7705033	mQTL is GWAS SNP	Visceral adipose tissue/subcutaneous adipose tissue ratio	22589738
rs2504567	chr6:26662913	rs1056667	0.90	Educational attainment	23722424
rs1405069	chr6:36922682	rs1405069	mQTL is GWAS SNP	Chemerin levels	20237162
rs71572559	chr6:66905309	rs3857536	0.88	Blood trace element	23720494

Supplemental Table 4: mQTLs in strong LD with GWAS SNPs

Five mQTLs are GWAS SNPs, and seventeen others are in LD ($r^2 \geq 0.8$ in YRI) with GWAS SNPs.

Assay	**CpG position**	**Primer names**	**Primer sequences**
Assay 1	chr1:196679457	HF CpG Assay_1 R1	/5BiodT/AT TTT CTA ACC CTT CAC CCT CCA TAA
		HF CpG Assay_1 F1	AGT GAG TAA AGG ATT TTA TGA TAT TGG
		HF CpG Assay_1 S1	AGG TTT ATA TGT TTA TTG TTT AGT
Assay 2	chr5:122774795	HF CpG Assay_2 R1	/5BiodT/AT TAC TAC TAC TTA CCA AAA ACT CTT AAA C
		HF CpG Assay_2 F1	GGA AAG GAA GTG AGG TAG TAA AA
		HF CpG Assay_2 S1	GAA GTG AGG TAG TAA AAA TAA TA
Assay 3	chr18:71774787	HF CpG Assay 3 R1*	/5BiodT/CA AAA CAA ACC ACT ATC CCA AAA T
		HF CpG Assay 3 F1	TGT TAT GGA GGT TTT GGT TTA ATA G
		HF CpG Assay 3 S1	GGA GGT TTT GGT TTA ATA GA
Assay 4	chr17:3089145	HF CpG Assay 4 F1*	/5BiodT/AG TGT TGG GAT TAT AGA TGT GAG TT
		HF CpG Assay 4 R1	ACC CTC TCC TCA AAC AAA TCT AAA TC
		HF CpG Assay 4 S1	AAA CTA TAT CTA CCT CCC
Assay 5	chr13:99923889	HF CpG Assay_5 R1*	/5BiodT/CA CTA TCC TAT CAA ACC ATT ATA CTA A
		HF CpG Assay_5 F1	TTG AGG GAG AAT TTG ATA ATT TGA GA
		HF CpG Assay_5 S1	AAA AGA ATG GGA AAT AAT GAA
Assay 6	chr21:30158046	HF CpG Assay 6 R1*	/5BiodT/TT CCC ACT TTA ACT CTT ACT TCA ATA CTA
		HF CpG Assay 6 F1	GAG TTA GAA ATT TAG GTT GGG TTT AGG
		HF CpG Assay 6 S1	TGT TTA TGT GTA GGG AAT
Assay 7	chr15:65164853	HF CpG assay_7 R1*	/5BiodT/CC TAC CAC CAC CCC TAA CTA ATT TTA TAT
		HF CpG assay_7 F1	AGA GGA AAT AGT AGG ATG TAA GTA GA
		HF CpG assay_7 S1	GGA GTT AGA GAT TAG TTT GGT TAA
Assay 8	chr20:61660870	HF CpG Assay 8 R1*	/5BiodT/TT ATC TTT CCT CAT TAA ACC TCT ACT
		HF CpG Assay 8 F1	GTT TTA GTT TTT TAG TTT GGA TTG GAT AA
		HF CpG Assay 8 S1	GTT ATA AGT TTT TTT TGG ATT TAG GG

Supplemental Table 5: Pyrosequencing primers

We used these primers for the pyrosequencing validation of mQTLs.